Progress in Quantum Electronics 75 (2021) 100303

Contents lists available at ScienceDirect

Progress in Quantum Electronics

journal homepage: www.elsevier.com/locate/pqe

Review

Strained-layer quantum well materials grown by MOCVD for diode laser application

Luke J. Mawst [a,*], Honghyuk Kim [a,e], Gary Smith [b], Wei Sun [c,f], Nelson Tansu [d,c]

[a] Department of Electrical and Computer Engineering, University of Wisconsin-Madison, Madison, WI, 53706, USA
[b] MIT Lincoln Laboratory, Lexington, MA, 02421, USA
[c] Center for Photonics and Nanoelectronics, Department of Electrical and Computer Engineering, Lehigh University, Bethlehem, PA, 18015, USA
[d] School of Electrical and Electronic Engineering, The University of Adelaide, Adelaide, SA 5005, Australia
[e] Now at Northwestern University, Evanston, IL, USA
[f] Now at II-VI Incorporated, USA

1. Introduction

Strained-layer quantum wells have revolutionized the performance of near-infrared diode lasers. Two primary factors leading to the prevalence of such materials are; 1) the ability for wavelength extension beyond that accessible from lattice-matched materials, and 2) the energy band-structure modification due to strain, leading to drastic reduction in transparency current densities. Semiconductor alloy compositions suitable for laser applications are generally constrained by the ability to synthesize either lattice-matched or pseudomorphic strained-layer quantum wells (QWs) on available substrate platforms. This has hindered the accessibility of certain wavelength regions, as well as the ability to fully exploit advanced heterostructure design. The compressively-strained InGaAs QW has become the workhorse for highly-reliable, high-performance lasers in the important 0.90–1.0 μm wavelength regime. Diode lasers employing such active regions have demonstrated the highest total power conversion efficiencies (70–76%) among all types of lasers. Nevertheless, many challenges remain to expanding the accessible emission wavelengths and addressing the associated strain-relaxation limitations of such material systems.

Highly-strained QW materials often consist of alloys which are metastable under conventional growth conditions. Such materials lie within the miscibility gaps of their equilibrium phase diagrams, but offer the potential to greatly expand the material platforms available for semiconductor lasers to enable higher performance and increase the span of emission wavelengths. While there is a wide range of metastable III/V semiconductor compounds available for diode lasers, we limit the scope of this review to less mature material systems which have significant challenges to reach full potential. High performance near-IR lasers employing metastable strained-layer $In_xGa_{1-x}As_yP_{1-y}$ QW materials grown on GaAs substrates have been developed for accessing the 0.70–0.78 μm wavelength region, as alternatives to conventional $Al_xGa_{1-x}As$-based QWs. To extend the laser emission wavelengths for GaAs-based devices into the telecom wavelength regions (1.3–1.55 μm), metastable materials such as $In_xGa_{1-x}As_yN_{1-y}$ and $GaAs_{1-z}Bi_z$ QWs have generated great interest. While high device performance has been achieved, many challenges remain in the synthesis and implementation of such materials into diode laser platforms. In particular, for manufacturing considerations such as high-throughput, the metalorganic chemical vapor deposition (MOCVD) process is generally the preferred method for the growth of semiconductor lasers. This review will focus primarily on MOCVD-grown materials and devices.

2. Strained-layer InGaAs quantum well 9xx-nm high-power lasers

2.1. Early strained-layer InGaAs QW lasers

During the mid-1980's three factors led to the fairly rapid development of strained-layer InGaAs quantum well (QW) lasers: (1) the

* Corresponding author.
E-mail addresses: ljmawst@wisc.edu (L.J. Mawst), gsmith@ll.mit.edu (G. Smith), nelson.tansu@adelaide.edu.au (N. Tansu).

https://doi.org/10.1016/j.pquantelec.2020.100303

Available online 5 November 2020

increasing use of precision epitaxial techniques to grow semiconductor crystals, (2) the investigation of the use of strained-layers in these crystals rather than just lattice-matched structures, and (3) the need for 980 nm pump lasers for erbium-doped fiber amplifiers (EDFAs) [1]. The drive by the telecom industry to increase communication capacity cannot be understated, as it drove hundreds of millions of dollars of investment to develop the pump lasers to enable wavelength division multiplexing (WDM) to use the full gain bandwidth of the EDFA.

The growth of strained-layer QW epitaxial structures in the mid-1980's was itself enabled by the introduction of molecular beam epitaxy (MBE) [2] and metalorganic chemical vapor deposition (MOVCD) [3] to controllably grow QW structures. Previous to the introduction of MBE and MOCVD, semiconductor heterostructures were typically grown by liquid phase epitaxy (LPE) which does not have the control necessary to reproducibly grow epitaxial structures at the nanometer scale. These epitaxial system improvements made during the 1970's and early 1980's enabled not only growth at the nanometer scale but precise compositional control to tailor the bandgap and lattice constant of the layers.

The use of strained-layer material was necessary to reach 980 nm, as the best-developed substrates to grow lattice-matched semiconductor lasers was fairly limited to GaAs and InP. InGaAs on GaAs substrates seemed a promising approach but in order to reach 980 nm, strains ($\Delta a/a$, where a is the lattice constant) of up to 1.5% would be needed. Fortunately, material scientists had been studying the critical thickness for layers of different lattice constants with other epitaxial materials. In particular, using the GaAsP-GaAs material system, Matthews and Blakeslee published the most commonly referenced paper that studied the elastic accommodation of strain in layers thinner than some misfit-dependent critical thickness [4]. They showed that a small amount of strain can be accommodated by the crystal without the formation of device-killing dislocations. Most importantly they derived a formula to calculate the critical thickness using readily available material parameters that have generally shown good agreement with results reported by subsequent groups.

By 1983, groups were attempting to grow and fabricate strained superlattice InGaAs-GaAs lasers but the devices failed within an hour [5,6]. Finally in 1984, Laidig et al. first published strained InGaAs QW lasers operating near 1 μm that survived 1000 h with less than a 25% increase in threshold current [7,8]. This soon drew many research groups to working in this area, as well as the attention of the telecommunications companies, and eventually a driving force of the telecom boom of the late 1990's.

Counterintuitively, strained QW lasers can actually improve the laser characteristics relative to lattice-matched semiconductor laser active regions, leading to these lasers holding the record for any laser with an efficiency at room temperature of an astounding 76% [9]. At the core of this improvement is the energy band structure of the semiconductor [10]. The biaxial compression present at the interface of strained InGaAs-GaAs heterostructures defeats the cubic symmetry of the semiconductor [11], splits the degeneracy of the heavy- and light-hole valence band edges [12], and reduces the in-plane effective mass of the heavy-hole band so that it assumes a light-hole like mass [13–15] (see Fig. 1). Yablonovitch and Kane showed that the lowering of the valence band effective mass to a value approaching the electron effective mass will reduce the injected carrier density necessary to reach lasing threshold [16,17]. Adams has also argued that the splitting of the valence bands reduces the two largest nonradiative recombination mechanisms: intervalence band absorption (IVBA) and Auger recombination, resulting in an increase in efficiency for strained layer lasers [18].

In the late 1980's and early 1990's, Coleman's group at the University of Illinois were the first group to publish detailed experimental results of a range of strained InGaAs-GaAs QW lasers for performance and reliability [19,20]. Beernink et al. reported the dependence of threshold current density on quantum well composition for a series of InGaAs-GaAs broad-area lasers with QW InAs compositions between 8 and 42%, all with a 7 nm QW width [19]. The relationship of these samples to the calculated critical thickness is shown in Fig. 2. Fig. 3 plots the resulting measured threshold current density for these broad-area lasers. The lowest threshold current density of 140 A/cm^2 is achieved for an InAs composition of 24%, with increasing threshold current density for higher InAs compositions attributed to approaching and exceeding the critical thickness (the lasers with $In_{0.42}Ga_{0.58}As$ QWs did not even reach lasing threshold).

In a second study, the QW InGaAs composition of the broad-area lasers was held constant at 25% InAs while the QW thickness was varied from 10 to 14.3 nm, crossing over the critical thickness as shown in Fig. 2 [20]. These lasers were placed on long-term aging tests

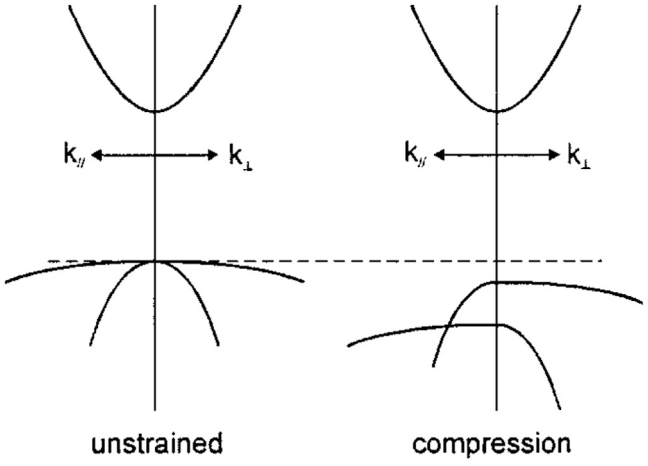

Fig. 1. E-k (energy-momentum) diagram of an unstrained direct semiconductor and a strained-laser semiconductor under biaxial compression [10].

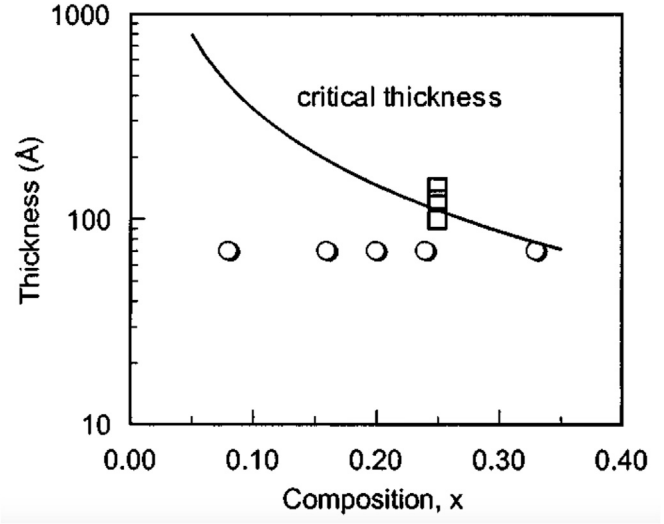

Fig. 2. Matthews and Blakeslee model calculated critical thickness (solid line) and $In_xGa_{1-x}As$ composition and QW thicknesses used in two experimental studies: (circles) study of threshold current density as a function of InGaAs composition with a 7 nm thick QW [19] and (squares) reliability study of InGaAs QW lasers near the critical thickness with a fixed InAs composition of 25% [20].

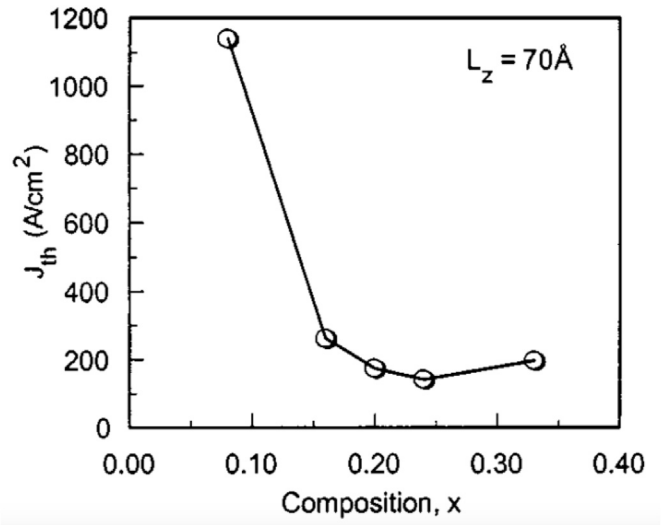

Fig. 3. Threshold current density as a function of QW composition for 150 μm × 815 μm devices with 7 nm $In_xGa_{1-x}As$ QWs [19].

at a constant output power of 60 mW and the current required to maintain that power measured as a function of time (Fig. 4). All of the 10 nm thick QW lasers survived the maximum time on test, while the 12.5 nm thick QW lasers showed some degradation. The 14.3 nm thick QW lasers, clearly well beyond the critical thickness, all failed within the first few hours of operation.

Within a short couple of years, the commonly held belief that strained-layer lasers were not reliable was completely turned on its head as it was soon shown by many groups that InGaAs-GaAs strained QW lasers were actually more reliable than similar lattice-matched GaAs-AlGaAs QW lasers. Dark-line defect (DLD) formation was already understood to plague the GaAs-AlGaAs lasers and lead to premature failures [21]. DLDs are a three-dimensional network of dislocations (dominated by nonradiative recombination) near the active region of the laser that propagates toward and eventually through the active region, causing failure. InGaAs-GaAs strained QW lasers were found to be resistant to this type of failure [22] and, in fact, the propagation speed of DLDs in the strained QW lasers was measured to be 1% of the speed in traditional QW lasers [23].

All of this groundbreaking work done in the late 1980's and early 1990's to demonstrate the performance and reliability of strained QW InGaAs/GaAs lasers set the foundation for two significant photonics industry booms in the coming decades: the telecommunications boom that started in the late 1990's then the laser materials processing boom that started around 2010 and is still thriving today, both of which will be discussed in the next two subsections.

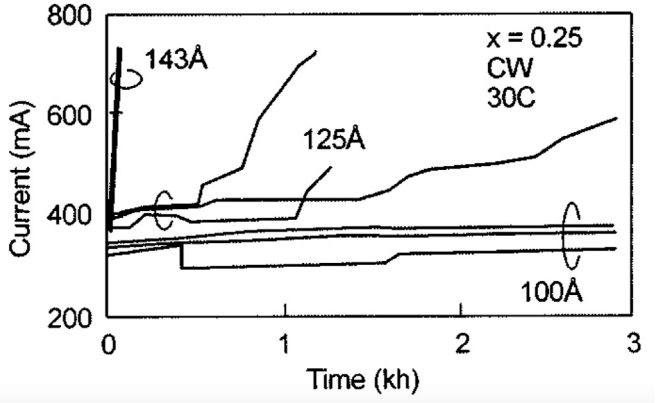

Fig. 4. Aging results for 60 μm × 600 μm broad-area $In_{0.25}Ga_{0.75}As$ QW lasers operating CW at 60 mW per uncoated facet at 30 °C [20].

2.2. Single-mode strained InGaAs/GaAs lasers spur the telecom boom

Single-mode 980 nm pump lasers were key to the telecom expansion in the late 1990's and early 2000's. Previous to using EDFAs, as telecom signals travelled through long-haul fiber-optic links they were attenuated by the fiber absorption so repeaters were needed every ~40 km to detect the laser data, electronically amplify it, and then retransmit it. The newly developed EDFAs instead just amplify the weakened signal thus eliminating the repeaters, which along with an increased in the spacing results in significant cost savings. Most importantly, EDFAs enabled the use of wavelength division multiplexing to have many channels of telecom data on the same fiber using transmission lasers with slightly different wavelengths, which was cost prohibitive with the repeater technology.

The initial work in strained InGaAs/GaAs lasers was primarily multi-mode, broad-area devices with typically ~100 μm wide emitters. These multi-mode lasers are not easily coupled into the ~6 μm mode-field-diameter single-mode optical fiber needed to core-pump the EDFAs being developed. Instead, single-mode lasers are needed with lateral waveguides that confine the optical mode to a ~5 μm waveguide. Both ridge-waveguide [24] and buried-heterostructure lasers [25] were investigated, but ridge-waveguide lasers won out for commercial development by most vendors due to the simpler process with higher yields, at least for GaAs-based lasers.

The next issue was the high-optical powers needed from the EDFA pump lasers, about 150 mW initially [24], from such a small aperture was not very reliable due to facet failures, which is different from the bulk dislocation-induced failures discussed in the last section where the failure was not near the laser facets. The problem was that exposing the AlGaAs active region to air formed native oxides that degraded the laser performance over time [26]. Researchers at IBM Zurich came up with a patented vacuum in-situ cleave and passivation process using a thin layer of silicon that was nicknamed the "E2 process" [27]. This process and similar processes developed by other groups [28–30] became standard to produce ever-higher-power pump lasers to satisfy the ever-increasing demand from the EDFA vendors for more power.

Facet passivation alone was not enough to get to the power levels that telecom vendors eventually demanded for their pump lasers. From the late 1990's to mid-2000's the reliable operating power from single-mode 980 nm pump lasers progressed from initially 150 mW up to over 1 W from a single device. The first strategy used was making the laser cavity longer, thus spreading out the heat in the laser [31,32]. Stretching the laser further to get higher power resulted in more facet failures though, so additional strategies were needed to reduce the power density and heating at the facet with many strategies used by different groups including: increasing the vertical mode size [33,34], using unpumped regions near the facet [33], disordering near the facet [35], non-absorbing mirrors [36], or flaring the ridge near the facet [37,38]. Today most of these methods are used in combination to achieve very-high-power single-mode lasers in excess of 1 W per emitter. An example of several generations of laser chips from one of these commercial vendors is shown in Fig. 5. The telecom industry still uses strained InGaAs/GaAs 980 nm pump lasers for EDFAs, but the larger semiconductor laser market today by far has moved on to multi-mode pump lasers for laser material processing, as will be described in the next section.

2.3. Multi-mode strained InGaAs/GaAs lasers fuel modern industrial lasers and laser weapon systems

Whereas telecom EDFAs are core-pumped fibers and require single-mode pump lasers, modern high-power industrial lasers use low-brightness multi-mode strained InGaAs/GaAs pump lasers. The workhorse industrial laser is the Yb-doped fiber laser which uses cladding mode-pumping rather than core-pumping as in EDFAs. The primary advantages to cladding-pumping are cost (multi-mode lasers are significantly cheaper on a per Watt basis) and thermal distribution (the pump is absorbed over a longer length of fiber, hence the waste heat from the pumping process is spread out). Yb-doped fiber can be pumped at the same wavelength as Er-doped fiber, ~980 nm, or a broader though less-efficient pumping at 915–940 nm – all with strained QW InGaAs/GaAs active regions. IPG Photonics has reported that the market for these pump lasers just for fiber lasers exceeds 100 MW of pump power produced per year [39], while the industrial laser business exceeds several billion U.S. dollars per year in revenue.

Increasing the power and efficiency of these multi-mode InGaAs/GaAs pump lasers has been paramount for decades, but was given a boost in the mid-2000's by the U.S. DARPA Super-High-Efficiency Diode System (SHEDS) program [40]. DARPA was interested in

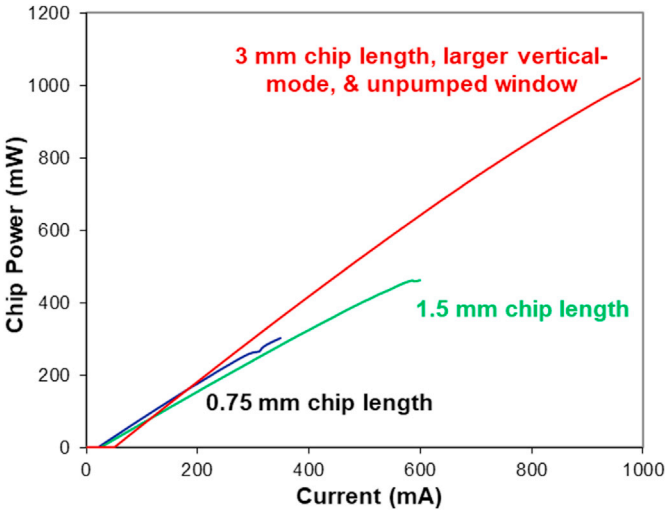

Fig. 5. Successive generations of commercial 980 nm pump laser chips from a commercial telecom pump laser vendor [32].

reducing the size, weight, and power (SWAP) of high-energy lasers (HELs) for weapon systems. A significant drawback to a diode-pumped solid-state HEL system at the time was the very low efficiency of 12.5% [40], with the pump lasers one of the largest single losses with their 45% efficiency. The program goal aimed to reach 80% diode pump efficiency after 3 years of investment from DARPA distributed to several competing commercial laser vendors [41–43]. Although they only reached 70–75% efficiency, it was still the single largest gain in efficiency in a few years period due to the significant investment by DARPA. At the same time as this DARPA program, IPG Photonics and Trumpf were investing heavily to develop fiber and disc lasers for materials processing, respectively [39, 44], which within a decade quickly blossomed into a multi-billion dollar industry. Meanwhile, the combination of fiber lasers with the high-efficiency pumps in particular spurred a high-profile U.S. Navy demonstration HEL weapon installed on the U.S.S. Ponce [45], which along with improvements in the technology have led to a current push by the U.S. DoD to develop deployed HEL weapon systems on multiple vehicle platforms [46].

In order to pump fiber lasers though, the power from these multi-mode emitters must be fiber-coupled. Although the fiber for these cladding-mode pumped fiber lasers is also multi-mode with typically 100–225 μm core fiber, the divergence of the beam in the slow-axis (the wide near-field dimension of the emitter which slowly diverges) can increase at the very high current densities needed to achieve the high powers resulting in decreasing coupling efficiency. This can be slightly improved by using a longer cavity length as shown in Fig. 6 [47], but that gain is insufficient since pump vendors want to push the power even higher. Many groups have studied this effect and the consensus agree that it is primarily a thermal lens effect [48] and several methods have been successfully employed to improve the slow-axis divergence increase [49,50]. This has resulted in a gradual increase of the state-of-the-art commercially available

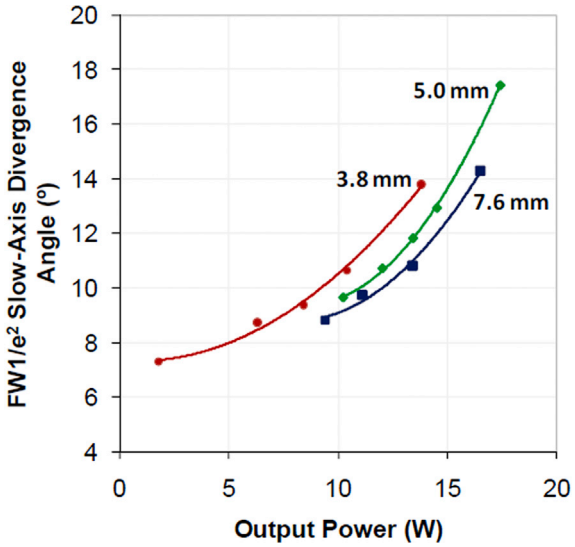

Fig. 6. Slow-axis divergence as a function of optical output power for a multi-mode pump laser at several different cavity lengths [47].

fiber-coupled reliable-operating power from about 8 to 10 W/emitter a few years ago [51] up to as much as 15 W/emitter today [49]. Meanwhile raw chip powers have been demonstrated with higher optical powers, as much as 27–30 W from a single-emitter [52,53], but powers are de-rated for long-term reliability by the pump laser vendors.

3. Highly-strained InGaAs quantum well active region lasers: wavelength extension

Expanding the materials platform for accessing long-wavelength emission on conventional GaAs or InP substrates will enable a variety of new high-performance laser architectures. For example, on GaAs substrates long-wavelength gain materials can then be monolithically integrated with high-index-contrast DBRs, to realize vertical cavity surface emitting lasers (VCSELs) for targeting telecom applications or visible sources (λ∼630 nm) via external frequency doubling. Furthermore, if efficient mid-IR (2–5 μm) sources and detectors could be produced on conventional InP substrates, this would represent a major technological breakthrough over existing interband cascade (IC) or type-I and type-II quantum well (QW) structures, which utilize more expensive GaSb or InAs substrates. Semiconductor lasers on InP substrates would have many advantages, including; access to a mature processing technology, better thermal conductivity, straightforward regrowth of buried-heterostructure type devices, and incorporation of buried distributed-feedback (DFB) structures. Although room temperature continuous wave (CW) operation has been achieved for InP-based quantum cascade lasers in the mid-IR, it is difficult to obtain high performance at wavelengths shorter than about 3.8 μm [54]. While shorter wavelengths are accessible using interband quantum well (QW) structures, traditional highly-strained InGaAs type-I multiple quantum wells (MQWs) [55–57] and InGaAs(Sb) type-I MQWs [58,59] on InP substrates are limited by strain relaxation to $\lambda < 2.1$ μm. In the InAs/InGaAs type-I MQW systems, the emission wavelength has been extended to 2.33 μm by employing very low temperature growth techniques [60,61].

Until the late 90's, InGaAs QW laser emission on GaAs substrates was generally limited to λ<∼1 μm [62]. The advent of strain-compensated InGaAs/GaAsP QWs combined with low temperature growth allowed for emission wavelengths to be extended to near λ ∼1.2 μm [63–65]. To extend the emission wavelength of the strained $In_xGa_{1-x}As$ QW beyond 1 μm on GaAs substrates, high-indium-content ($x > 0.2$) QWs are necessary, which exhibit large compressive strain. Ultimately, the longest emission wavelength achievable from an InGaAs QW grown on a GaAs substrate is limited by the strain relaxation from the lattice mismatch between the QW layer and substrate. The (strain) x (thickness) product of the QW active region is a key factor governing the degree of strain relaxation, and thus the radiative efficiency of the material. Recent studies on the reliability of highly-strained InGaAs QW lasers also point to a link between reliability and strain x thickness product [66], similar to what was observed earlier by Coleman for lower indium-content InGaAs QW lasers [67]. There is an inherent tradeoff between the dominate competing factors for achieving lower transition energies; quantum size effects and compressive strain both shift the emission to shorter wavelength, while increased indium content reduces the bandgap and enables longer wavelength emission. These factors all contribute to the expected emission wavelengths, shown in Fig. 7, for highly-strained QWs.

3.1. Growth considerations

Unlike typical MOCVD growth conditions (∼750 °C) used for the laser cladding and waveguide layers, the highly-strained InGaAs QWs need to be grown at relatively low growth temperatures (<550 °C). Lower growth temperatures were found to improve luminescence efficiency, attributed to the reduced strain-relaxation through the formation of misfit dislocations [63,68–70]. At a reduced

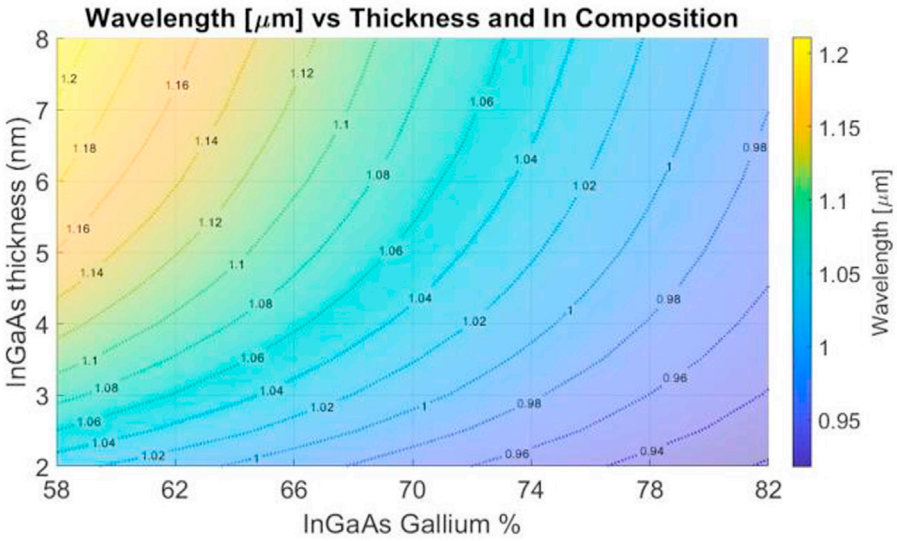

Fig. 7. Simulated emission wavelength for highly-strained InGaAs QWs with varying Ga content and QW thickness.

temperature, the surface energy during the growth is also lowered compared to the energy to form strain dislocations, which will in turn increase the effective critical thickness of the materials [71,72]. In addition, maintaining a 2D growth mode is important to avoid strain relaxation at the edges of island formation at the growth surface. Kinetically inhibiting the formation of 3D islands by minimizing mass transport at the growth surface can be accomplished by using low growth temperatures, high growth rate, and high V/III ratio [65].

It was shown by Ekenstedt et al. in 1995 that the critical thickness of the InGaAs on GaAs is a strong function of substrate temperature during the growth, with lower substrate temperature resulting in larger effective critical thickness [72]. The room temperature photoluminescence intensity is an effective means to gauge the degree of strain relaxation of the InGaAs QW. Schlenker et al. [65], used this method to verify that InGaAs QWs with strain-thickness products well beyond that predicted by Mathews and Blakeslee critical thickness model are possible with appropriate growth conditions [73] (see Fig. 8).

The large compressive strain of the high-indium-content InGaAs QW can be compensated by employing tensile-strained GaAsP barriers [63,74]. Since the average strain of the QW plus barriers can be designed to be near zero, this technique is particularly attractive for the growth of MQW active regions. In addition, the use of $GaAs_yP_{1-y}$ tensile-strained barriers provide a higher potential barrier than can be provided by a GaAs barrier. The larger band offset between the barrier and the QW will lead to reduced carrier leakage out of the QW, and a lower temperature sensitivity of the threshold current density and also the external differential efficiency of the diode lasers [75].

Recent studies have also identified that the strain-compensated QW structures have improved structural and optical properties compared with highly-strained QWs without strain-compensating barriers [76]. A significant amount of strain relaxation (~1.53%) is identified by X-ray diffraction reciprocal space mapping (RSM) when the thickness of each $In_{0.4}Ga_{0.6}As$ QW within a 4-period multiple quantum well (MQW) structure approaches to 9.5 nm in the absence of strain-compensating layers. Inserting ~5 nm-thick $GaAs_{0.67}P_{0.33}$ tensile-strained barriers into these MQW structures reduces the strain relaxation down to ~0.3% and improves surface roughness. A specific elastic energy density of the tensile-strained barrier has been identified to be essential to achieve optimal strain compensation in an heavily-strained InGaAs MQW structure.

Nine different designs of strain compensated $In_{0.4}Ga_{0.6}As/GaAs_{1-y}P_y$ MQW were studied by Sun and Kim et al. Those designs have the same 9.5 nm $In_{0.4}Ga_{0.6}As$ well layer and were categorized by different *P*-content (group A: $y = 0.15$; group B: $y = 0.25$; group C: $y = 0.33$), and different thickness of the $GaAs_{1-y}P_y$ layer (group 1: 5 nm; group 2: 7.5 nm; and group 3: 10 nm). The strain relaxation and outcomes in PL and surface morphology were compared to two conventional 9.5 nm $In_{0.35}Ga_{0.65}As$ MQW (R3) and $In_{0.4}Ga_{0.6}As$ MQW (R4).

When the In-content in the conventional 9.5 nm InGaAs MQW increased from 35% to 40%, the InGaAs layer exceeds its critical thickness based on People and Bean model [65,77]. Accordingly, the RSM plot in Fig. 9 shows a dramatic change in the lateral separation of GaAs peak and MQW fringe peaks, suggesting a large strain relaxation of ~1.53% in MQW. In contrast, with GaAsP tensile barrier incorporated, the strain relaxation was suppressed to ~0.3%, comparable to that for the $In_{0.35}Ga_{0.65}As$ MQW. Such evolution in strain relaxation is also reflected on the micro-PL mapping and surface morphology of the MQWs. It is clear to see that the effect of strain compensation depends on the design of the GaAsP tensile strained layer. As the *P*-content and thickness varies, the total elastic strain energy *W* also changes, given the relation in Ref. [78]:

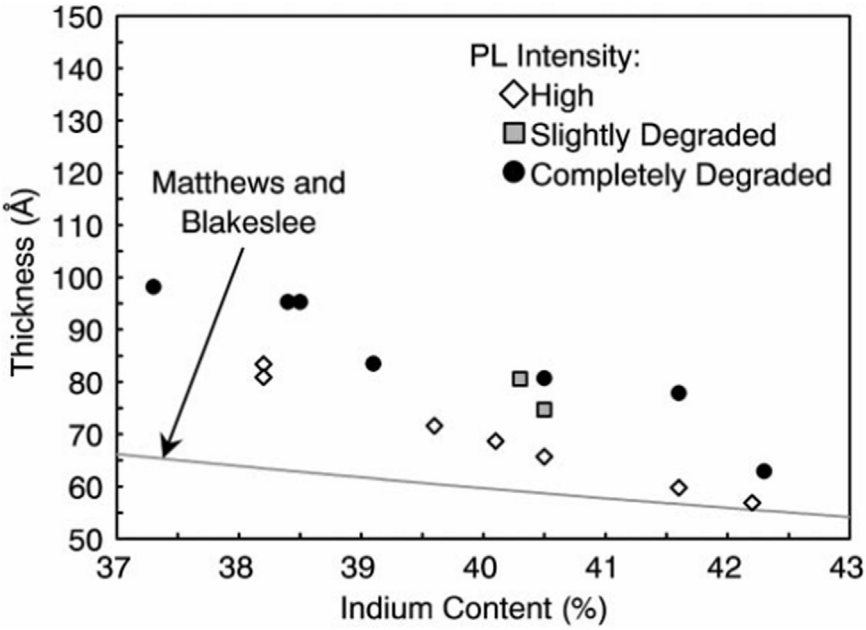

Fig. 8. Comparison of experimental data indicating relative PL intensity for InGaAs QWs grown at low temperature with varying indium content and thickness. For reference, the solid line show the calculated critical thickness based on the Matthews-Blakeslee model. Adopted from Schlenker et al. [65].

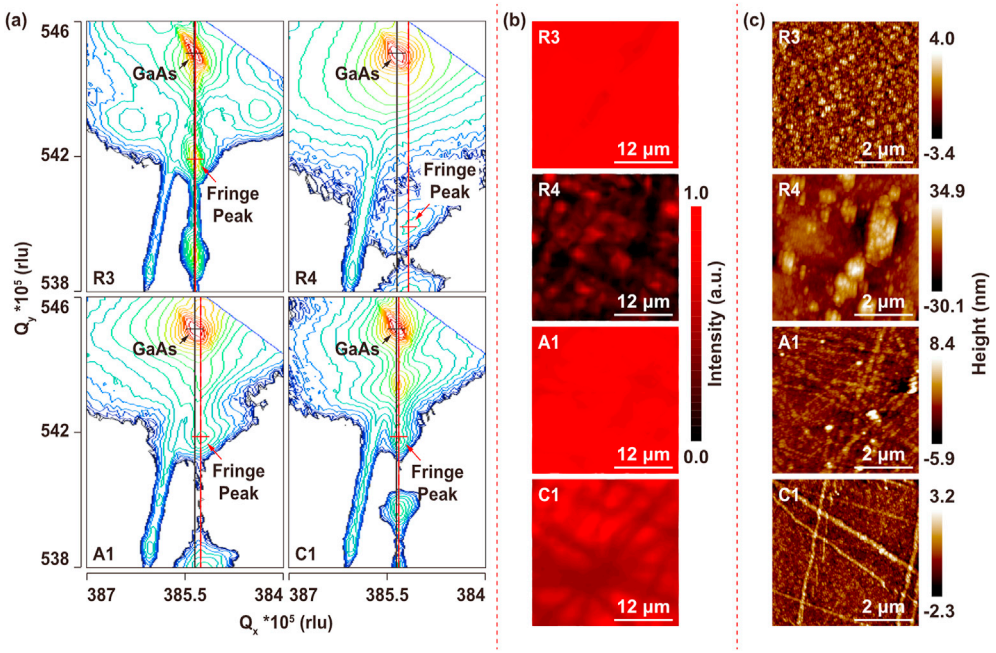

Fig. 9. **(a)** XRD RSMs along (224) direction, **(b)** micro-PL mapping, and **(c)** AFM between the conventional $In_xGa_{1-x}As$ MQWs (R3, x = 0.35 & R4, x = 0.4) and strain-compensated $In_{0.4}Ga_{0.6}As$ MQWs with $GaAs_{1-y}P_y$tensile barriers (A1 and C1).

$$W = l\left(C_{11} + C_{12} - 2\frac{C_{12}^2}{C_{11}}\right)(\varepsilon_{xx})^2$$

where l is the $GaAs_{1-y}P_y$ layer thickness, and ε_{xx} is the strain tensor in the $GaAs_{1-y}P_y$ layer with respect to GaAs substrate. The C_{11} and C_{12} are the elastic stiffness constant. From the plot of strain relaxation against the elastic energy density in $GaAs_{1-y}P_y$ tensile strained barrier (Fig. 10), the strain relaxation is first reduced and then recovered as the energy density increases. Thus, a valley was identified giving the favorable range of elastic energy density in the GaAsP layer for a given InGaAs MQW (in this case, 9.5 nm $In_{0.4}Ga_{0.6}As$).

This study suggested a potential direction of the optimization of strain compensation to achieve favorable active region design. On the other hand, the current study was still limited by the characterization techniques. The characterization of strain relaxation using RSM tool is suffering from averaging effect due to large X-ray beam spot. Any variation in layer thickness and composition could potentially affect the precision especially at near-pseudomorphic condition. Moreover, this study was assuming that the strain is evenly distributed within each strained layer, which require further investigation using advanced characterization tool. Thus, we would expect more precise measurement to conduct statistical examination to reveal the optimal correlation between tensile barriers and strain compensation, which will be of great interests for high performance laser diode using highly strained InGaAs MQW.

3.2. Device performance

High performance lasers with total power conversion efficiencies exceeding 70% have been demonstrated in the 0.9xx-μm emission wavelength regime, through material growth and heterostructure design optimization [79–81]. However, highly-strained InGaAs QW devices have not realized such performance levels, with total power conversion efficiencies of ~50% being demonstrated at wavelenths of 1150 nm [82]. This may stem in-part from material property degradation for highly-strained quantum wells grown under non-optimal conditions required to kinetically inhibit strain relaxation. Nevertheless, ultra-low threshold current density lasers in the λ = 1.1–1.2 μm wavelength regime have been reported by a number of groups [69,75,83–89].

Tansu et al. employed a highly-strained 6 nm-thick $In_{0.4}Ga_{0.6}As$ QW ($\Delta a/a = 2.78\%$) with $GaAs_{0.8}P_{0.2}$ barriers to demonstrate ultra-low threshold current densities J_{th} of 90A/cm^2 at 1233 nm for cavity lengths of 1 mm. The strong active region carrier confinement lead to a low temperature sensitivity for the slope efficiency, T_1 = 1250 K [83]. Wavelengths as long as 1.26 μm have been reported for highly-strained InGaAs MQW active region lasers, although threshold current densities (J_{th} ~350A/cm^2) are increased as the wavelength exceeds ~1.24 μm [85]. The comparison of the threshold current density in Fig. 11 shows the extension of emission wavelength above 1.24 μm increased the threshold current density up to 1.8 kA/cm^2, which clearly indicates the need for strain compensation or other new active regions with a more balanced strain consideration.

Optical gain and radiative efficiency studies on highly-strained InGaAs QW lasers provide insights into degree of nonradiative carrier recombination processes present as the critical thickness is approached. The peak optical gain as a function of current density can be extracted from a conventional cavity length analysis, (CLA). These gain-current relationship from experiment is often fitted to a phenomenological dependence, Eq. (1).

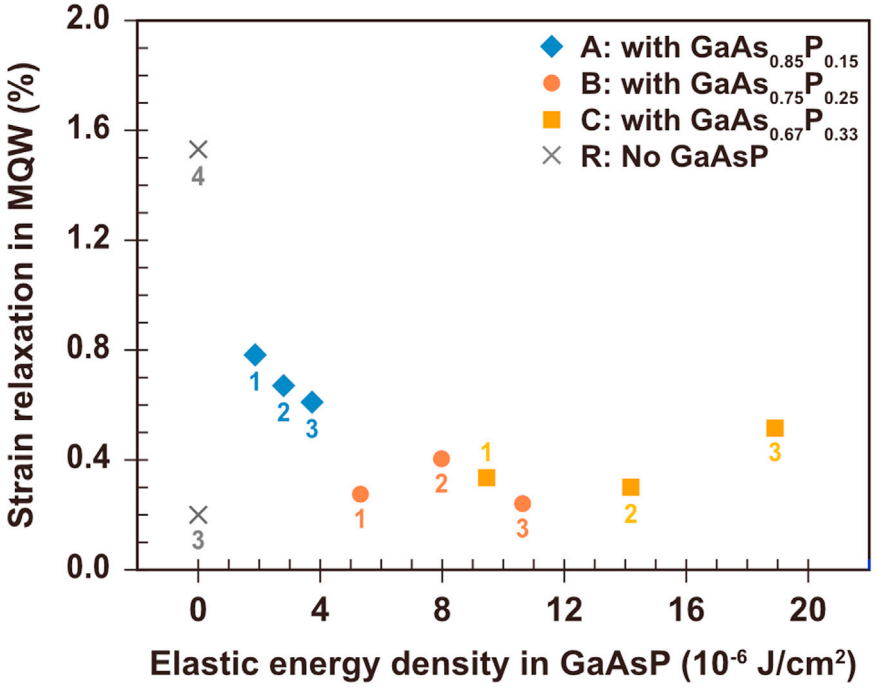

Fig. 10. Strain relaxation in $In_xGa_{1-x}As$ MQWs versus the elastic energy density in the $GaAs_{1-y}P_y$ barrier for strain-compensated $In_{0.4}Ga_{0.6}As$ MQWs and the $In_xGa_{1-x}As$ MQWs (R3, x = 0.35 and R4, x = 0.4) with no strain-compensation.

$$G_{m,\max} = g_0 \ln(J_{tot} / J_{tr}) \tag{1}$$

$G_{m,\max}$ denotes material gain spectra maximum [90,91], g_0 and J_{tr} are the material dependent gain parameter and transparency current density, respectively.

It is instructive to compare the gain properties of high-performance 0.98 μm-emitting (8.5 nm-thick) $In_{0.2}Ga_{0.8}As$ QW with that of a highly-strained 1.2 μm-emitting lasers which contain an active region consisting of a 6-nm thick $In_{0.4}Ga_{0.6}As$ QW (Δa/ã2.5%) [92]. The highly-strained QW material displays a larger gain parameter, g_0, and lower transparency current density, J_{tr}, as shown in Fig. 12. The lower transparency current density is expected because of the equalization of the conduction and valence band density of states [93,94].

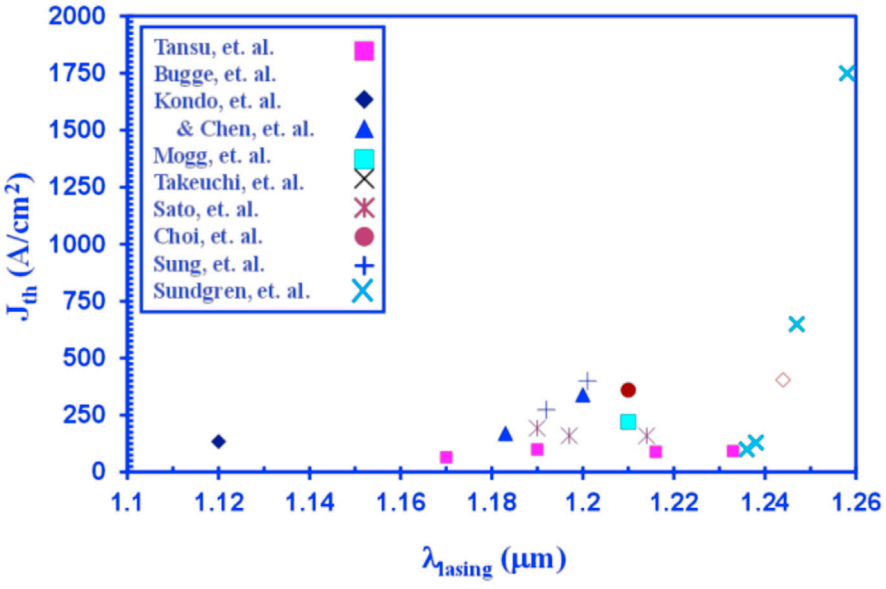

Fig. 11. Comparison of threshold current densities for highly-strained InGaAs QW lasers as a function of emission wavelength.

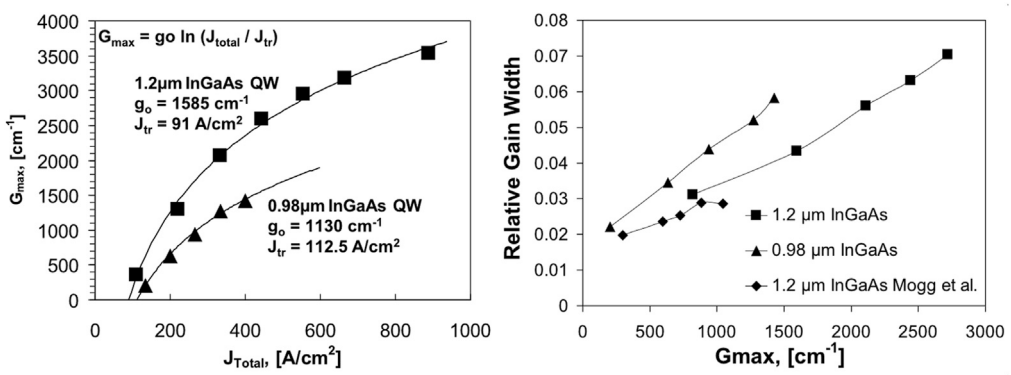

Fig. 12. (a) Comparison of the measured peak gain, G_{max}, as a function of injected current density for conventional 0.98 μm-emitting QW lasers and highly-strained 1.2 μm-emitting lasers, (b) Compariosn of the measured relative spectral gain bandwidth for conventional 0.98 μm-emitting QW lasers and highly-strained 1.2 μm-emitting lasers.

The compressive strain reduces the density of states, which is expected to lead to a reduction in the $g_0$value, although other factors such as differences in QW width and emission wavelength, and the spectral width of the gain also influence the value of g_0.

In order to assess the role of nonradiative recombination in these lasers, multi-segment amplified spontaneous emission (ASE) measurements [95] can be useful for extraction of the inherent "radiative efficiency" of the QW active layer materials, and provide information not obtainable from other conventional materials characterization techniques. For a given total current injection, the carrier concentration in the active region is determined by the injection efficiency, which is a complex function of the carrier leakage and recombination lifetimes. However, carefully-designed experiments can be useful in extracting a detailed picture of the recombination mechanisms and carrier leakage effects in these structures. ASE measurements have been utilized to measure spectral gain and radiative efficiency characteristics of highly-strained InGaAs QW lasers, and compare these properties with those from lower-strain, λ~0.98 μm, InGaAs QW lasers [96] (Fig. 13). The measured ASE characteristics are determined as a function of total injected current density. At each injection level, the *radiative* current density can be determined from the integrated spontaneous emission spectra. Comparing the values for radiative and total current density allows us to understand the various nonradiative recombination and leakage pathways in these laser structures. These insights are invaluable in the further optimization of the laser structures and shed light on the optical properties of these highly-strained active region materials.

Since the ASE measurement allows us to extract the spontaneous emission spectra, which can then be integrated to obtain the radiative current density, the peak material gain can also be plotted against the *radiative* current density, as shown in Fig. 13 a). Note that the radiative part of the transparency current density for the highly-strained InGaAs QW is extremely low, J_{tr_rad} = 11.2A/cm^2, indicating that significant improvement in device performance is possible if nonradiative recombination can be further reduced. Comparing the radiative current density to the total current density, the ratio yield the radiative efficiency of the structure, as shown in Fig. 13 b). It's interesting to observe that the radiative efficiency of highly-efficient 0.98 μm-emitting InGaAs QW lasers have J_{rad}/J_{total} of <50% [97]. However, note that we cannot directly obtain information on the true radiative efficiency or "internal spontaneous radiative efficiency" of the QW, since to do this we need to first know what fraction of the injected current is lost through recombination outside the quantum well (i.e. what is the value of the current injection efficiency, η_{inj}). Note that the value of η_{inj} is structure dependent and in general difficult to determine below laser threshold, corresponding to the ASE measurement conditions.

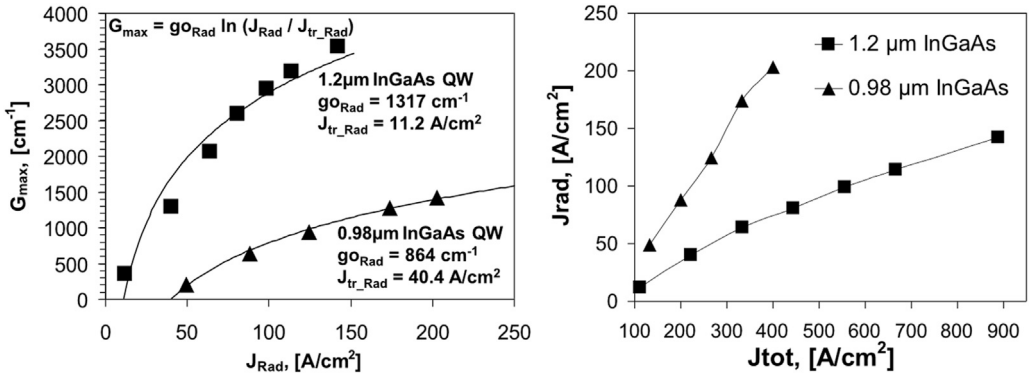

Fig. 13. Comparison between highly-strained and lower-strain QW lasers using data extracted from multi-segment device measurements; a) measured material gain vs. radiative current density, b) radiative current density vs. total current density.

3.3. Reliability considerations

The importance of the link between the strain-thickness product of the InGaAs QW active region and reliability was demonstrated by Coleman [67]. Even though high-performance devices can be realized above the theoretical critical thickness limitations on the QW active region, long term reliability may degrade. At 1120 nm wavelengths, either thicker GaAs barriers to decouple the strain in an MQW, or GaAsP barriers were found to be effective to allow for reliable operation at multi-watt output powers near RT [66]. In addition, strain introduced by the AlGaAs cladding layers can influence the reliability for devices operating near the strain x thickness product limit. This issue was previously identified by Tansu et al. where a strain compensating buffer layer was employed for the growth of the highly-strained 1.2 μm-emitting InGaAs QW on a high-aluminum-content AlGaAs cladding layer [74]. Such devices exhibit some degree of degradation after 500 h at a constant output power of 100 mW at room temperature, as shown in Fig. 14. Clearly, challenges remain to achieving high-output-power (Watt-range) long term reliable operation at $\lambda \sim 1.2$ μm wavelengths.

3.4. Type-II approaches for targeting 1.3 μm on GaAs

In a type-I QW, the longest emission wavelength achievable is limited by the (*strained*) bandgap energy of the QW material. For example, in the InP-based material system, the conventional approach of using a highly-strained $In_xGa_{1-x}As$ QW, encounters difficulties for wavelength extension beyond λ~2 μm, due to strain relaxation. By contrast, a type-II QW such as the InGaAs/GaAsSb QW structure on an InP substrate, removes this constraint and allows for spatially indirect electron-hole recombination to occur with a corresponding transition energy which is *smaller* than the energy bandgap of either the InGaAs (electron well) or the GaAsSb (hole well). The primary drawback of such a structure is that there is reduced spatial overlap (i.e. reduced optical matrix element) of the electron and hole wavefunction, compared with that of a type-I QW. In addition the spatial charge separation in a type-II QW leads to a built-in electric field with a magnitude that depends on the carrier density. This built-in electric field generally results in an undesirable blue-shift that is carrier density dependent, so that the emission wavelength may strongly depend on the threshold gain. In general, to accurately predict the emission wavelength in a type-II QW laser, the carrier dependent charge separation needs to be accounted for.

Type-II QWs on GaSb substrates have also been extensively researched and incorporated into mid-IR laser structures. The type-II InGaSb/AlSb W-structure was proposed [98] and first implemented on a GaSb substrate, as a means to optimize the electron-hole wavefunction overlap and retain a two-dimensional density of states. Interband Cascade Lasers (ICLs) [99,100] employing type-II QWs can be designed for laser emission over a wide wavelength range ($\lambda = 3$–6 μm) within the mid-IR spectral region [101,102]. Type II QW structures also provide for reduced Auger recombination, one of the primary mechanisms leading to the strong temperature sensitivity of long wavelength lasers, as reported by Bewley et al. [103]. It is notable that to date, all GaSb-based ICLs have been grown by MBE. However, the use of MOCVD for the growth of Type-II QW active region lasers has been demonstrated in other material systems, such as GaAs and InP. The MOCVD growth of thin layer superlattices containing $GaAs_{1-y}Sb_y$ layers is complicated by the surface segregation of Sb-atoms and the As-for-Sb exchange reactions at the interface between the alternating layers [104]. The incorporation of Sb in epitaxial $GaAs_{1-y}Sb_y$ films is also challenging due to a large thermodynamic miscibility gap manifested for the GaAs-GaSb binary alloy system, generally requiring low temperature growth conditions and optimized interface gas switching conditions [105,106]. On an InP substrate, both InGaAs and GaAsSb can be engineered to have either tensile or compressive strain. This provides a large design space for accessing long-wavelength emission into the mid-infrared region. Such MOCVD-grown InP-based type-II QW lasers have been realized by Peter et al. employing a superlattice active region consisting of compressively-strained InGaAs and tensile-strained GaAsSb, with room temperature lasing observed up to 1.71 μm [107]. The design and MOCVD growth of strain-compensated type-II

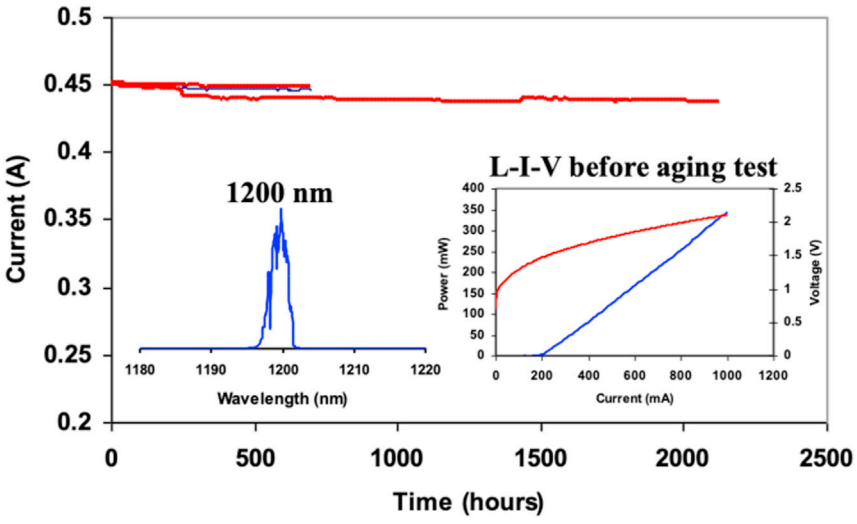

Fig. 14. Constant power (100 mW) burn-in for several InGasAs QW lasers emitting at 1.2 μm.

InGaAs/GaAsSb W-type active regions were reported by Huang et al. [108], and RT photoluminescence at ~2.1 μm was observed from type-II 'W' structures containing $In_{0.8}Ga_{0.2}As$ (~4.0 nm)/$GaAs_{0.35}Sb_{0.65}$ (~1.5 nm) QWs bounded by InP (5 nm) spacer layers and $AlAs_{0.77}Sb_{0.23}$ (1.5 nm) barrier layers. Optimization of the optical matrix element, for a given emission wavelength, is necessary for maximizing the optical gain. Note that the simulation results shown in Fig. 15 do not include the effects of injected carrier density, which is expected to result in a blueshift of the emission wavelength with increasing carrier densities.

More recently, using MBE growth, room temperature lasing was reported up to 2.55 μm from type-II InGaAs/GaAsSb W-type active regions [109]. By contrast, conventional type-I QW lasers on InP are limited to wavelengths less than about 2.33 μm, due to strain relaxation of the high indium content InGaAs active region [59,61].

By contrast, GaInAs/GaAsSb type-II QWs on GaAs substrate are inherently compressively-strained. Such structures have been employed to extend the emission wavelength of GaAs-based sources into the telecommunication range ($\lambda = 1.3–1.55$ μm) [110–113]. Low threshold current density lasers (610A/cm^2) grown by MOCVD employing such active regions were first reported by Dapkus et al., although emission wavelengths were limited to 1.2 μm [112]. More recently, relatively low threshold current density laser operation (1 kA/cm^2) has been reported for devices operating near 1.3 μm, which hold promise for realizing long wavelength VCSELs on GaAs. Further extension of emission wavelength on GaAs can be anticipated if metastable material systems, such and dilute-nitrides or dilute-bismides, can be utilized in conjunction with the type-II W structures [108,114–119].

4. Metastable strained-layer QW materials

4.1. Phase separation and growth challenges: InGaAsP on GaAs substrates

The quaternary InGaAsP material system grown on InP substrates has been firmly established as the material of choice for long-wavelength near-infrared lasers in the telecom bands (1.3–1.55 μm), even though under certain growth conditions such materials are metastable and have shown compositional phase separation [120]. While less-mature metastable materials, such as dilute-nitride and dilute-bismide alloys, show promising potential, they have not commercially replaced the well-established InGaAsP material system. InGaAsP alloys grown on GaAs substrate have also found application for shorter wavelength near-infrared sources ($\lambda < 1$ μm), so called Al-free material system. However, a large portion of the available InGaAsP compositional range on GaAs substrate falls well within the compositional miscibility gap under conventional MOCVD growth temperatures. Semiconductor diode lasers with emission wavelengths in the 0.70–0.78 μm range traditionally employ either very thin GaAs QWs [121,122], or relatively high-aluminum-content (In) $(Al_xGa_{1-x})As$ ($x > 0.15$) QW active regions [123–126]. However, several factors make the reliability of AlGaAs-active layer devices challenging within this wavelength regime; 1) sensitivity to fabrication induced defects and susceptible to dark-line defect propagation into the active region, 2) bulk defects or oxygen contiamination introduced during growth, 3) and facet oxidation and degradation. Since the AlGaAs QW active region has a high surface recombination velocity, exposed (oxidized) AlGaAs surfaces at the facet were found to lead to catastrophic optical mirror damage (COMD) at low optical power densities [127,128]. However, the development of sophisticated facet passivation technologies, such as, for example the non-absorbing mirror (NAM) [129–133] or E2 process [134], provide complete facet passivation and largely eliminate this facet degradation issue. Nevertheless, bulk degradation remained an underlying issue aggravated for higher-aluminum-content active regions. Bulk degradation associated with unintentional impurities and non-radiative recombination centers, such as oxygen, are present in the active-layer material. Pioneering work by Roberts et al. to employ in-line purification of the metalorganic reagents used in the MOCVD process, demonstrated that oxygen contamination can be reduced in AlGaAs short wavelength lasers and improved device reliability was observed [135]. Later studies, demonstrate that the use of low-oxygen MOCVD sources can produce watt-level reliability in the 0.70–0.78 μm wavelength region [136]. An alternate approach, which is to eliminate the highly reactive aluminum (Al)-containing compounds from the active region, has also been an effective method to reduce bulk degradation in diode lasers, and allow for high-power watt-level reliable operation in the 0.7–0.78 μm wavelength region [137]. These Al-free metastable InGaAsP/GaAs materials also provide more flexibility over AlGaAs, by allowing for either tensile- or compressively-strained active regions for optimization of device performance or polarization control.

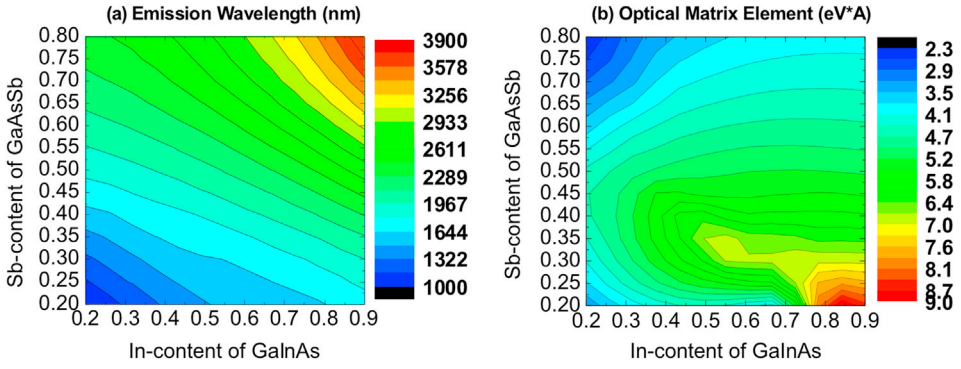

Fig. 15. Compositional design space for type-II InGaAs (2.5 nm)/GaAsSb (2.5 nm) W-structures on InP a) emission wavelength, b) optical matrix element. Adopted from [108].

The quaternary InGaAsP lattice-matched to GaAs falls between the ternary (InGaP) and binary (GaAs) compositional endpoints, with corresponding energy bandgaps in the range $E_g = 1.9–1.42$ eV. The growth of this quaternary on GaAs is challenging because of the existence of a miscibility gap occurring at typical MOCVD growth temperatures (650–700 °C) for compositions which fall within the mid-energy-gap region (i.e. $E_g = 1.65–1.7$ eV) [138–141]. Compositional phase separation resulting from the immiscibility leads to a significant broadening of the room-temperature PL and poor surface morphology [142]. Lattice-mismatch strain is expected to modify the compositional phase diagram and the alloy solubility, although the impact of compositional phase separation on the properties of strained-layer InGaAsP QWs and device performance is not well established. MOCVD growth techniques have been developed which utilize kinetic processes to control nucleation and suppress mass transport during growth, resulting in reduced compositional phase separation. For example, the use of low temperature growth [143] and modification of the surface steps by using mis-cut substrates [144, 145] has been effective means to reduce compositional phase separation for InGaAsP materials. Below, we focus on QW materials allowing for emission wavelengths $\lambda < 0.8$ μm, since these quaternary materials fall well within the immiscible compositional region for typical MOCVD growth conditions.

Tensile-strained InGaAsP or GaAsP QW active regions have been reported for the 0.7–0.8 μm wavelength region [146–148]. The laser separate confinement heterostructure (SCH) designs consist of either a AlGaInP waveguide region with AlInP cladding layers [146], or AlGaAs waveguide and cladding layers [147,148] to provide optical and carrier confinement. High *P*-content GaAsP QW active layers (i.e. higher tensile strain) results in emission wavelength as short as 0.715 μm [147]. However, weak (hole) carrier confinement results in excessive carrier leakage, reflected in the low values for the characteristic temperature coefficients for threshold current density and slope efficiency; T_0 and T_1 values of 60 K and 110 K respectively near $\lambda = 0.735$ μm. Nevertheless, reliable RT operation at 2 W CW was demonstrated from these Al-free active structures employing Large Optical Confinement (LOC) waveguide AlGaAs layers with 1–2 μm thickness [149]. Such an LOC design results in reduced optical power density at the laser facet (i.e. large d/Γ value, where d is the quantum well width and Γ is the optical confinement factor) and a narrow transverse beam divergence. Reducing the optical power density at the laser facet, by employing a d/Γ ~1, increases the maximum output power possible without encountering catastrophic optical mirror damage (COMD). However, since these GaAsP active regions don't contain indium, they may be more susceptible to dark-line defect propagation into the active region, compared with InGaAsP QWs [150].

Diode lasers emitting near $\lambda = 0.73$ μm employing $In_{0.48}Ga_{0.52}As_{0.4}P_{0.6}$ compressively-strained (Δa/ã1.65%) 15 nm thick QWs, which fall deep within the miscibility gap (see Fig. 16), have been reported by MOCVD on a highly-misoriented substrate (10° towards <111>A) [144]. Reduced photoluminescence linewidths were observed from the InGaAsP QW, possibly due to improved miscibility of the quaternary material when grown on the misoriented substrate. More recent studies on bulk films grown by MOCVD confirm that mis-cut substrates towards (111)A lead to reduced phase separation and improved surface morphology. Tensile-strained (Δa/ã-0.75%) 10 nm InGaP QW barrier layers were employed to improve carrier confinement and provide partial QW strain compensation, see Fig. 17. The use InGaP barrier layers, together with the use of high bandgap $In_{0.48}(Ga_{0.5}Al_{0.5})_{0.52}P$ cladding/waveguide layers for the laser provides strong active region carrier confinement, and results in relatively large T_0, T_1 values of 115 K and 285 K respectively. Such lasers have demonstrated Watt-range CW operation with minimal degradation [137] and have more recently been commercialized as single-mode sources [151].

4.2. Dilute-nitride QW materials

4.2.1. Dilute-nitride active region lasers

Given the inherent wavelength limitations of InGaAs/GaAs QWs dictated by strain relaxation, other material systems are needed to extend laser emission wavelengths longer than ~1.2 μm on GaAs substrates. Proposed by Weyers et al. [152] and Kondow et al. [153], dilute-nitrides materials such as GaAsN and InGaAsN open up new opportunities to realize low cost, high performance 1.3–1.55 μm

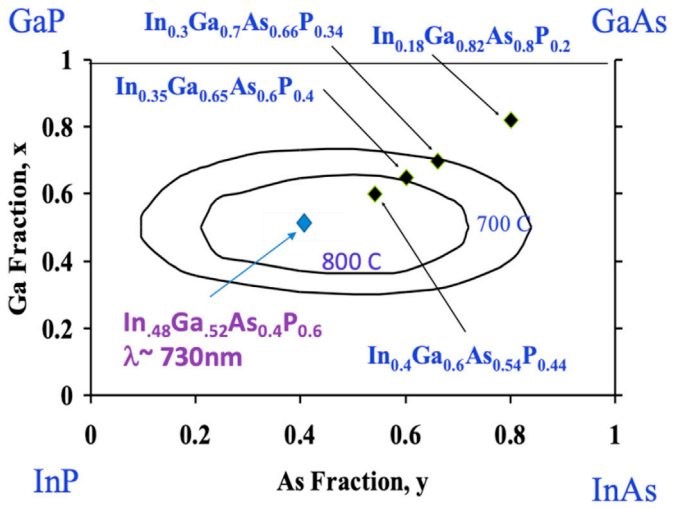

Fig. 16. Miscibility gaps as a function if growth temperature for InGaAsP alloys.

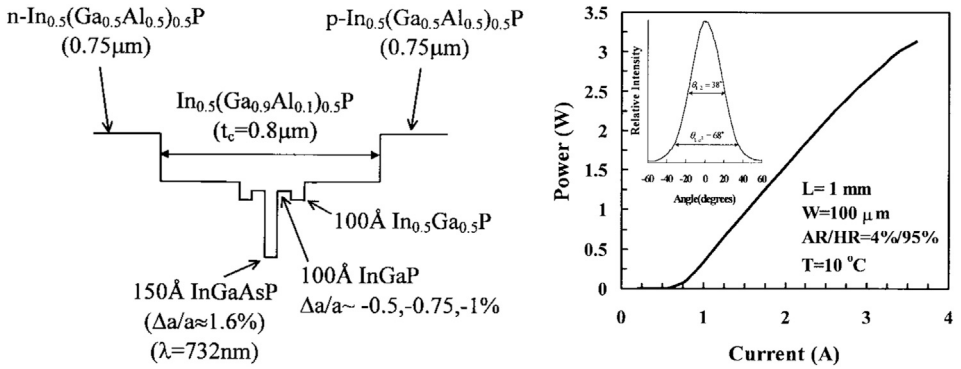

Fig. 17. (Left) Schematic diagram of 730 nm-emitting laser structure employing a compressively strained InGaAsP QW with compositions falling within the miscibility gap shown on Fig. 16. (right) CW output power characteristics for broad stripe 730 nm-lasers. Adopted from Refs. [144].

emitting semiconductor diode lasers grown on GaAs substrates. Dilute-nitride QWs grown on InP substrates, or metamorphic buffer layers, allow for emission wavelengths into the mid-infrared spectral region (>2 μm). While the potential of the dilute-nitrides for lasers is enormous, it is challenging to grow these metastable materials with high crystalline perfection and sufficient optical properties as required for device applications. These materials generally suffer from structural nonuniformities and exhibit low radiative efficiency, nevertheless high performance devices have been demsonstrated by both MBE and MOCVD through optimization of growth conditions.

The band anticrossing model has been used to show that the presence of N in InGaAs produces a localized resonant energy level that interacts with the conduction band [154]. The electronic coupling between this resonant N level and the conduction band splits the conduction band, and results in a drastic reduction in the lowest energy bandgap (ΔE_g ~100 meV/%N for N< 3%). The small atomic size of N compared to As also results in a reduction in the crystal lattice parameter, as shown in Fig. 18, which decreases the amount of compressive strain for a given indium content InGaAs alloy and allows for lattice-matched InGaAsN films to be grown on GaAs substrates.

High-indium-content (x~0.4, y~0.01) $In_xGa_{1-x}As_{1-y}N_y$ QWs with $GaAs_{0.8}P_{0.2}$ barriers, grown on GaAs, can achieve 1.3 μm laser emission wavelengths for typical quantum well widths of ~ 8–10 nm, as shown in Fig. 19. The use of GaAsP barriers were found to be key in reducing the strain relaxation and suppressing the carrier leakage especially the hole leakages attributed to the larger valence band confinement.

Dilute-nitrides exhibit a wide miscibility gap in their phase equilibria, making N incorporation thermodynamically unfavorable, so that epitaxial growth is determined by kinetic processes [155]. The solubility on N into these alloys is extremely low, generally requiring low growth temperatures and high growth rates to incorporate sufficient N for device applications. This leads to variations in materials grown by different techniques, i.e. MOCVD and MBE, and has led to difficulties in determining the fundamental nature of these materials and the role of growth-technique-specific defects. Consequently, these materials problems have somewhat hindered device design and fabrication.

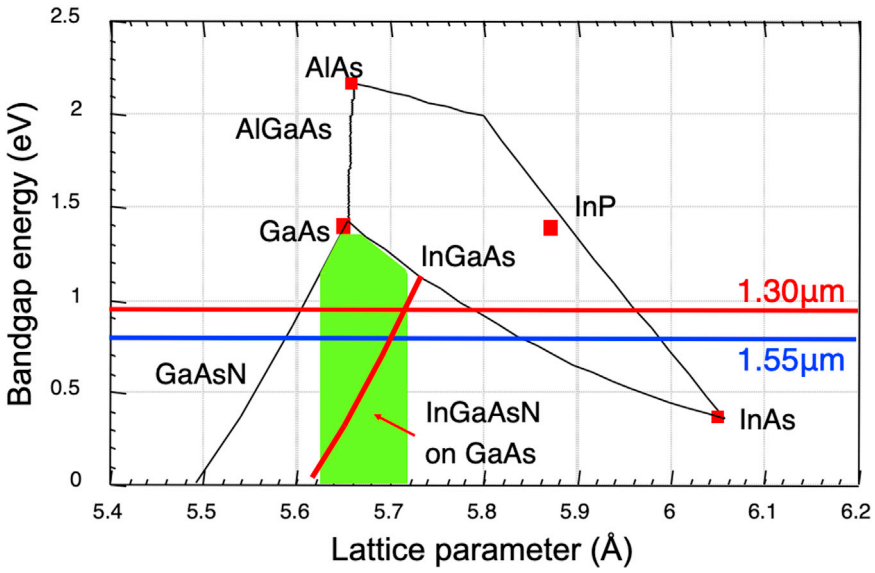

Fig. 18. Energy bandgap vs. lattice parameter for various III/V semiconductors, including GaAsN and InGaAsN on GaAs.

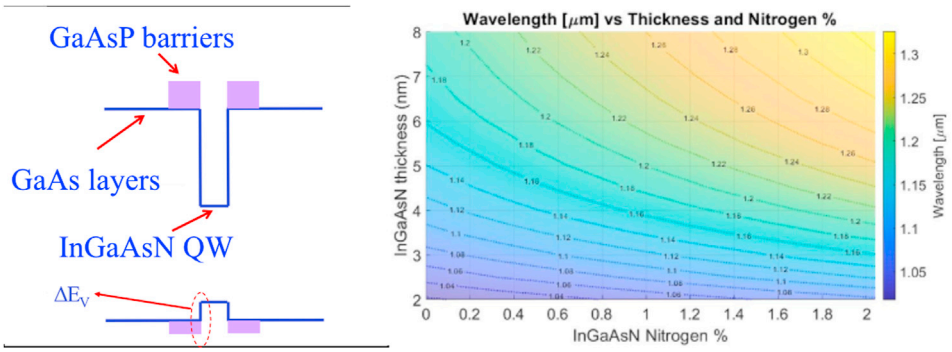

Fig. 19. (Left) Schematic diagram of InGaAsN QW with GaAsP barriers; (right) Simulated photoluminescence (PL) wavelength based on a 10-band k*P model for an $In_{0.4}Ga_{0.6}As_{1-y}N_y$ QW with $GaAs_{0.8}P_{0.2}$ barriers with varying N content (y) and well thickness. Note that the lasing wavelength is typically blue-shifted with respect to the PL emission.

All dilute nitride materials studied to date exhibit a drastic reduction in minority carrier lifetime (and minority carrier diffusion length) with increasing N content. *N*-related defects result in large (nonradiative) monomolecular recombination, which spoils the optical material quality. In-situ and/or ex-situ thermal annealing or current annealing has been found to be effective in improving the optical properties of dilute-nitride materials on GaAs substrates [156,157]. In addition to deep level traps [158], introduced by *N*-incorporation, other annealing dependent issues have been identified in dilute-nitride materials such as hydrogen incorporation [157, 159,160], variability of the nearest neighbor nitrogen configuration [161], and built-in local strain fields [162,163]. Fig. 20 shows the comparison of the effect of *N*–H-V_{Ga} complexes on the device characteristics of InGaAsN QW lasers. When the devices were cooled down under a H_2/AsH_3 environment, then the effect of current annealing (Fig. 20) is dramatic, resulting in a process by which electrical injection removes the defect complexes. Initially, the source of this current annealing effect was unclear, but the subsequent experiment by replacing the H_2/AsH_3 cool down step with a N_2 only cool down removes the current annealing effect and reults in stabilized low threshold current devices.

The use of the N_2 cool down during the growth of InGaAsN results in the reduction in the *N*–H-V_{Ga} complexes. Fig. 21 shows the comparison of the H-level in secondary ion mass spectroscopy (SIMS) data for both cooling down mechanisms, indicating that the N_2 cool down results in an H-level of 1×10^{19} cm^{-3} in the active region which is about 2.5 times lower than that of the sample cooled down under H_2/AsH_3. In addition, because dilute-nitrides are grown by MOCVD at relatively low temperatures (<550 °C), unintentional high carbon incorporation is observed. The SIMS data shown in Fig. 21 indicates a *C*-level of 3–4x10^{17} cm^{-3} for both cases. Increasing the growth temperatures can reduce the carbon background doping, although at the expense of N incorporation efficiency [164,165]. The optimization of MOCVD-grown InGaAsN materials and an understanding of growth limitations are essential to further optimizing these materials.

Early studies of InGaAsN-active lasers utilized relatively high nitrogen concentrations ~2–3%, leading to very high threshold current density lasers (>1 kA/cm^2) [153]. As for highly-strained InGaAs QWs, employing low growth temperatures allowed for higher-indium incorporation into the InGaAsN QW, without strain relaxation, thereby requiring smaller amounts of nitrogen to achieve 1.3

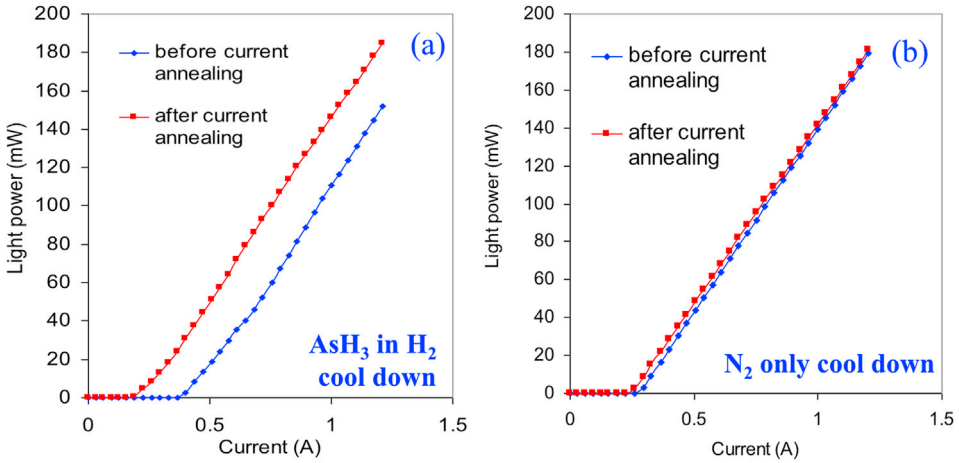

Fig. 20. The comparison of the light output power versus current for diode lasers with strain-compensated InGaAsN QW with GaAsP barriers with two cooling down mechanisms in the reactor. The data for devices which was grown under cooled down with (a) AsH_3 in H_2 and (b) N_2 only are presented. The results are compared for both before and after current annealing.

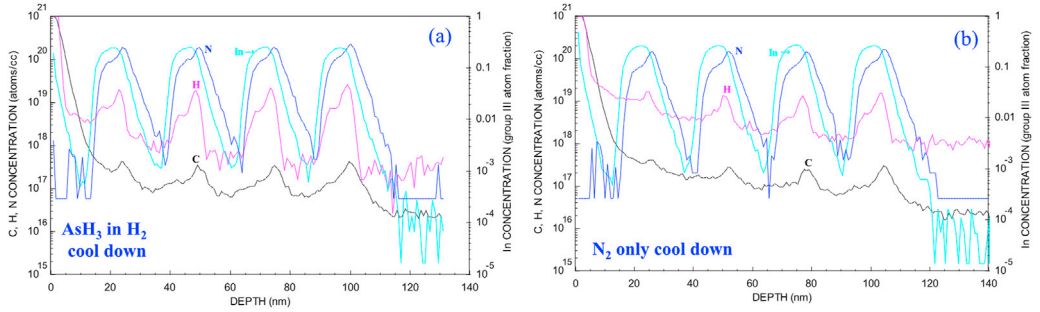

Fig. 21. Secondary ion mass spectroscopy (SIMS) analysis of various elements including H, N, C, In for InGaAsN active region cooled down under (a) AsH_3 in H_2 and (b) N_2 only.

μm-emission. InGaAsN QWs with lower nitrogen content (~0.5%) in the InGaAsN-active region, resulted in significantly improved threshold current densities (0.225 kA/cm^2) [166]. The low temperature sensitivity of these InGaAsN lasers, allows low threshold current density CW operation at high temperature and high CW output powers (1.8 W). Higher CW output powers (8 W), as well as stable operation at 1.5 W CW for over 1000 h at 35 °C has been reported for MBE-grown devices [167]. Reliability studies on MOCVD-grown InGaAsN QW lasers have not yet been published.

In contrast to the InGaAsP-InP QW laser which generally utilize a large number (9–14) of wells, the InGaAsN QW lasers require only a single QW active region for high temperature operation, owing to the larger material gain parameter and better electron confinement in the QW. As a result, the 1.3 μm InGaAsN single-QW diode lasers, with cavity lengths of 500 μm, have threshold current densities of only 940 A/cm^2 at a heat-sink temperature of 80 °C. Longer cavity length devices (L_{cav} = 2000-μm) at temperatures of 80 °C exhibit threshold current densities of only 455 A/cm^2 under CW operation [166]. By comparison, 1.3 μm-emitting InGaAsP-InP QW lasers exhibit threshold current densities of approximately 1650–1700 A/cm^2 for devices with cavity-length of 500-μm at operation temperature of 80 °C [168].

One challenging goal remaining for dilute-nitrides is to extend the emission wavelength beyond 1.3 μm, while maintaining optical material quality for the realization of longer wavelength, high-performance, GaAs-based devices. While there have been reports of low threshold current density InGaAsSbN QW [169] and InGaAsN [170] QW active lasers grown by MBE in the 1.5 μm wavelength region (see Fig. 22), this performance level has not been achieved by MOCVD. It is notable that while this device performance is impressive for 1.5-μm emitting lasers grown on GaAs substrate, the highest performance at these wavelengths is still obtained from devices structure with more conventional material on InP [171].

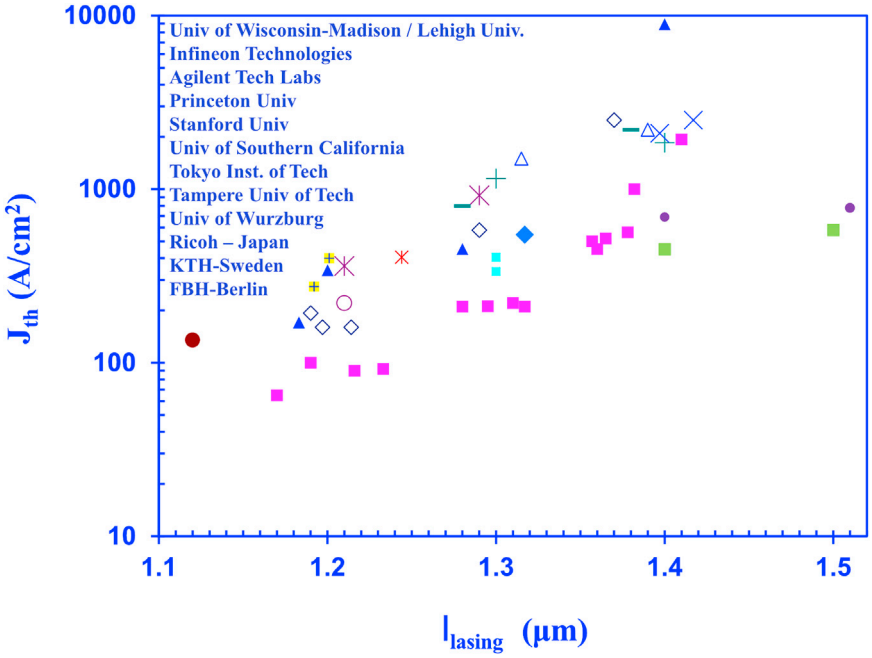

Fig. 22. The comparison of the threshold current density for dilute-nitride-based InGaAsN and InGaAsSbN quantum well lasers grown on GaAs substrate. The data were obtained from numerous groups with varying cavity lengths and device structures [1.5 μm-emitting data points from 169, 170].

The general trend observed by many research groups of increasing threshold current density with longer emission wavelength, along with a corresponding higher N content, is evident from Fig. 22.

While the origin of the N penalty on threshold current density for MOCVD-grown InGaAsN is believed to stem from nonradiative (monomolecular) recombination, the specific defect complexes and effective means to eliminate these defects by growth optimization is not well established. However, many device studies have been reported which provide insights into the specific impact of N on laser performance. Studies on 1.3 μm-emitting InGaAsN QW lasers indicate that the current injection efficiency, η_{inj} (T), is more temperature sensitive than 1.2 μm-emitting InGaAs QW lasers, which results in a highly temperature sensitive external differential quantum efficiency, η_d, and reflected in low T_1 value [172]. This increased temperature sensitivity of the η_{inj} is believed to result from carrier (hole) leakage. The use of higher bandgap GaAsP QW barrier layers was found to be effective to improve carrier confinement and lead to an increased T_1 value [75]. A high T_1 valve, indicating a temperature insensitive η_d, is important for high output power CW operation, since self-heating under CW operation can lead to a drastic drop in efficiency if the T_1 value is low. Carrier leakage as well as nonradiative processes, such as monomolecular recombination and Auger recombination [173] lead to a reduction in the material gain parameter g_{0J}, with N incorporation [75]. In addition, a reduction of the effective differential gain by 1.6–2 x compared to InGaAs QW lasers has been confirmed by RIN [174] and modulation response measurements [175 and 176].

While dilute-nitride materials have been studied extensively as a means to extend the emission wavelength of GaAs-based sources into the near-IR (λ = 1.3–1.55 μm), relatively less work has been reported on dilute-nitride materials and devices for emission and detection in the mid-to long–wavelength infrared spectral region (λ∼3–15 μm). GaSbN [177,178], InGaAsSbN [179], and InAsN [180] can potentially access wavelengths in the range of 3–15 μm, provided sufficient N can be incorporated into the alloys. However, as discussed above, the *N*-related defects result in large (nonradiative) monomolecular recombination, which spoils the optical material quality. However, at present little is known about how these issues impact mixed Sb/N alloys for mid-IR or LWIR emission. One such dilute-nitride material with strong potential for mid-to LW-IR emission is InAsN. Early work on InAsN demonstrated a bandgap energy reduction with increasing nitrogen content (∼29.6–31meV/%N [181,182]), although the materials exhibit broad photoluminescence (PL) at low temperatures. $InAs_{0.97}N_{0.03}$/InGaAs/InP multiple quantum well laser structures were first reported in 2001, emitting at 2.38 μm, although threshold current densities were quite high (3.6 kA/cm^2) and devices only operate up to 260 K [183]. Strong PL emission at 4.5 μm from $InAs_{0.975}N_{0.025}$ and InAsSbN alloys grown by MBE were also reported [184,185]. Employing a InP_ySb_{1-y} or $InAs_yP_{1-y}$ graded composition metamorphic buffer layer (MBL) provides an additional means to control the active region strain and required nitrogen content in the QW active region, and allows for growth on an InP substrate [186,187]. Note that a reduction of the compressive strain of the InAsN QW, by employing an MBL, will lead to significant wavelength extension.

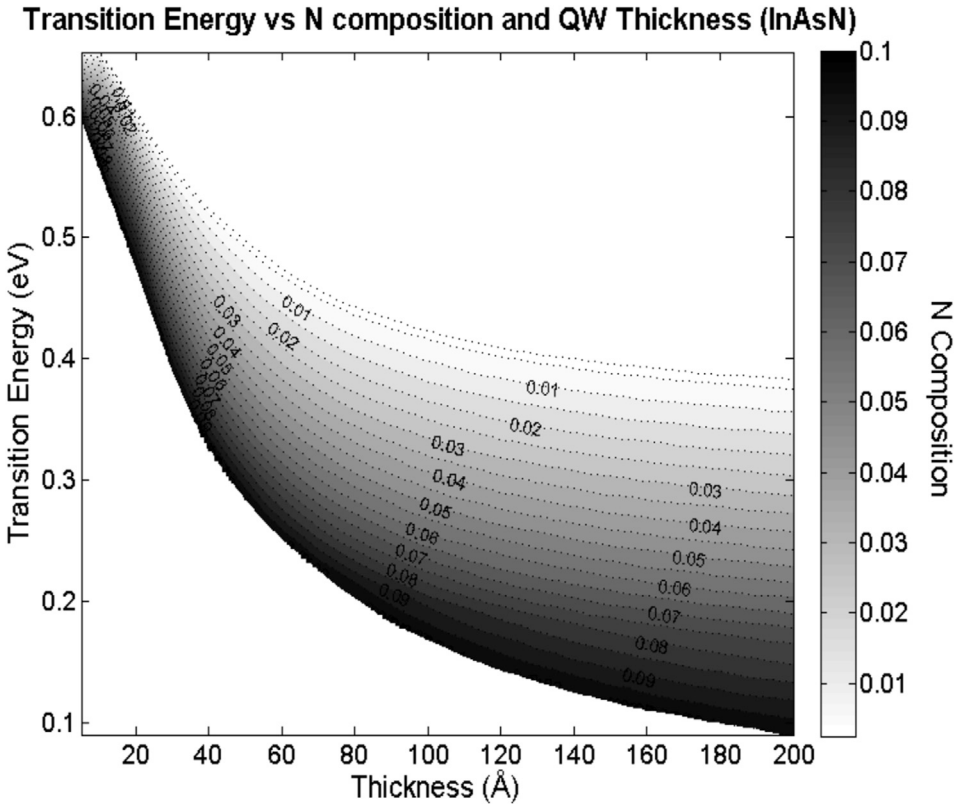

Fig. 23. Calculated emission wavelength using a 10-band k*p model for an $InAs_{1-x}N_x$ QW as a function of nitrogen content and quantum well thickness grown on top of the compositionally-graded InAsP MBL structure with a lattice constant of $InAs_{0.5}P_{0.5}$ The nitrogen content is shown as the contour value.

10-band k*p simulations indicate that an emission wavelength of over 4 μm can be achieved from a 15 nm thick $InAs_{0.97}N_{0.03}$ QW (Δa/ã 0.8%) grown on such an MBL, as shown in Fig. 23.

MBE grown InAsN QW structures incorporating an MOCVD-grown $InP_{1-y}Sb_y$ MBL on InP has been used to achieve room temperature emission, as shown in Fig. 24 [188]. The MBL consists of 10-step compositionally-graded $InP_{1-y}Sb_y$ (y = 0.0–0.2) terminating with an $InAs_{0.5}P_{0.5}$ (500 nm) capping layer [187].

While these developments demonstrate that mid-IR emission up to room temperature is readily achievable with bulk InAsN and InAsSbN on InAs substrates or on MBLs on InP, additional work is needed to develop the growth of QW structures employing these materials, to implement the QWs into device structures and determine the optimal (post-growth) thermal annealing conditions. Furthermore, the incorporation of N into InAs is challenging by MOCVD, due partly to the weak indium-nitrogen bond.

4.2.2. Effect of strain on the nitrogen incorporation in dilute-nitrides

The growth of dilute-nitride InGaAsN with high In-content (~40%) on GaAs and InP results in compressive and tensile strain films, respectively. The use of high In-content InGaAsN on GaAs is necessary for accessing into the longer spectral emission regime. Under the compositional range of interest for photonics applications, the *N*-incorporation into InGaAsN on GaAs was studied under the compressive strain state. In contrast, the pursuit of dilute-nitride InGaAsN on InP will be primarily grown under a tensile strain condition. Initial studies were conducted for InGaAsN with In-content of 40% under the identical growth conditions on both GaAs and InP substrates, and the nitrogen incorporation efficiency into the films are found to be dramatically different. This finding points out the strong dependence of the nitrogen incorporation efficiency into the dilute-nitride layer on the strain state of the layer. Prior studies have also been reported on the strain-dependent N incorporation efficiency [189].

The growth of InGaAsN with In-contents of 35% and 40% on GaAs substrates results in compressively strained host materials. The typical MOCVD growth conditions for InGaAsN used [DMHy]/V molar ratio of ~0.95–0.99, which corresponds to an approximately 0.5% up to 2% *N*-incorporation into the active layer materials. The growth temperatures were carried out at 530 °C with H_2 carrier gas. To illustrate this, Fig. 25 shows the SIMS data for an $In_{0.35}Ga_{065}AsN$ QW with a thickness of 8-nm. The host material has a compressive strain of +2.45%. The [DMHy]/V molar ratio used for this experiment was 0.961. The X-ray diffraction measurement confirmed the *N*-content as 0.8% based on the lattice distortion from the nitrogen incorporation into the film. The SIMS data clearly showed that a distinct *N*-peak within the QW with an intensity of two orders of magnitude lower than that of the In-peak; this is consistent with the XRD data.

In contrast, the InGaAsN QW with similar In-contents (35–40%) grown on an InP substrate resulted in a tensile strained host material. By using the same range of [DMHy]/V molar ratio of ~0.95–0.99, the following experiments were carried out on InP substrates. For consistency, an identical growth temperature (530 °C) and pressure (200 mbar) were employed, and the In-contents varied from 20% up to 50% in the host materials. Fig. 26 shows the SIMS data for the tensile-strained $In_xGa_{1-x}AsN$ QW grown on InP with In-contents from 20% up to 50% under [DMHy]/V molar ratios of (a) 0.961 and (b) 0.981. The thickness of the QWs were ~6 nm, and the tensile strain of the host QWs was −1%. The nitrogen incorporation into the solid phase of the InGaAsN/InP was found to be less than 0.001%, which corresponded to 6-order of magnitude lower than that of the In-content in the QW. The increase in [DMHy]/V molar ratios from 0.961 to 0.981 only marginally increased the nitrogen content in the QW. The lack of nitrogen incorporation in the solid phase of the QW is also verified by the lack of any shift in the peak wavelength of the photoluminescence of these samples. As a comparison, under similar growth conditions with an In-content of 40% resulted in 0.5% and 0.8% *N*-contents in the compressively-strained $In_{0.4}Ga_{0.6}AsN$ QW

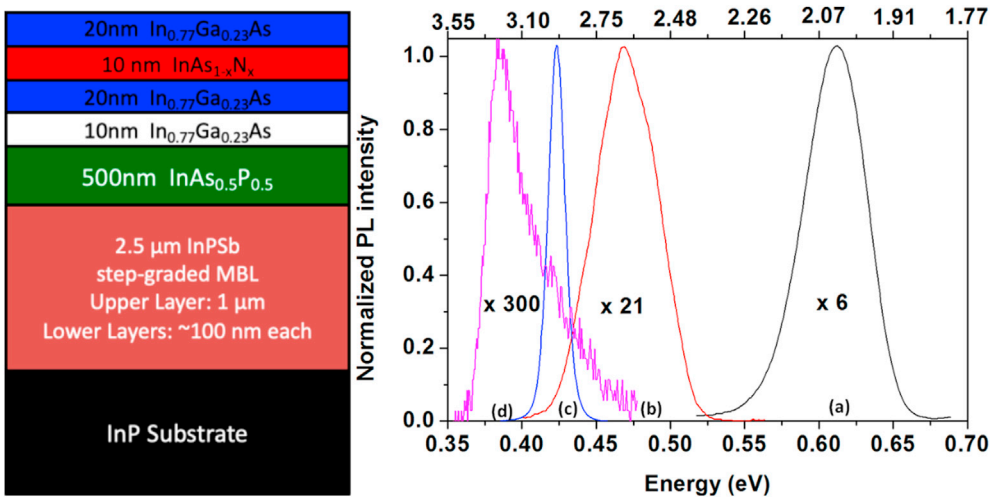

Fig. 24. (Left) Schematic diagram on $InAs_{0.99}N_{0.01}$ on InPSb graded composition MBL, (right) 4 K PL spectra from InGaAsN samples on InP substrate (a) 1% N (black), (b) 2% N (red), and (c) 1% N on MBL (blue); (d) is the normalized 300 K PL spectrum of sample (c) [Adopted from 188].

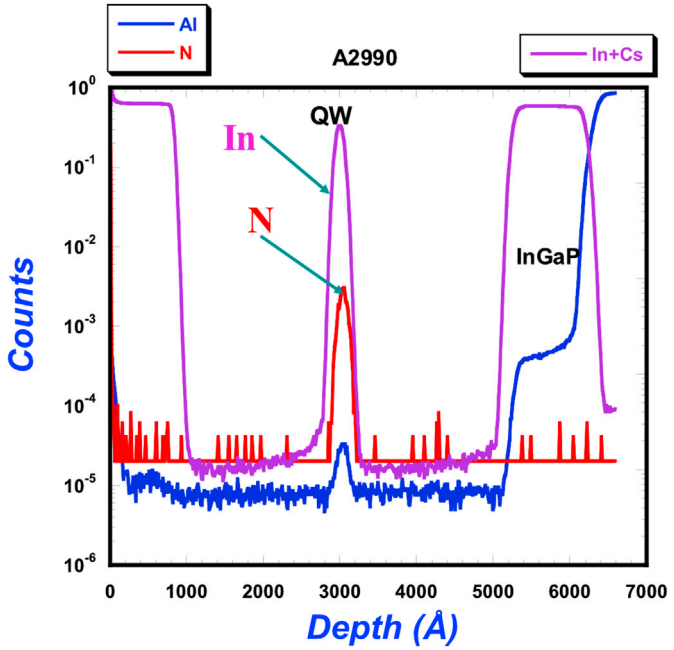

Fig. 25. SIMS measurement of $In_{0.35}Ga_{0.65}AsN$ QW layer grown on a GaAs substrate with a [DMHy]/V molar ratio of 0.961. The QW host material was grown under compressively-strained state.

grown on GaAs for [DMHy]/V molar ratios of 0.961 and 0.981, respectively. This finding strongly suggests a distinct incorporation efficiency of the nitrogen in solid phase for compressive- and tensile-strained InGaAsN QW layers, which opens up the needs to investigate further this phenomenon at the fundamental material science levels for enabling device implementation.

4.2.3. Type-II dilute-nitride QWs for wavelength extension

Dilute-nitride-based type-II QWs on InP also have potential as mid-infrared wavelength sources. Such an active region design consists of an InAsN-GaAsSb type-II multiple-quantum-well (MQWs) active region utilizing the modified 'W'-shape transitions [115], with built-in *strain-compensation, strong carrier-confinement,* and *large electron-hole overlap*. Similar type-II QW structures on InAs substrates were also proposed by Debbichi et al. for accessing the 3 μm wavelength region [190]. Such type II QW active regions may lead to reduced Auger coefficient and IVBA to increase efficiency and also improve hole confinement leading to higher power room temperature operation. The band diagram for one period of the dilute-nitride structure with 0.30-eV energy gap (λ = 4.1 μm emission) at room temperature is shown in Fig. 27. Each of the two $InAs_{0.97}N_{0.03}$ (2.6% compressive strain) electron QWs are 12 Å thick, and the single

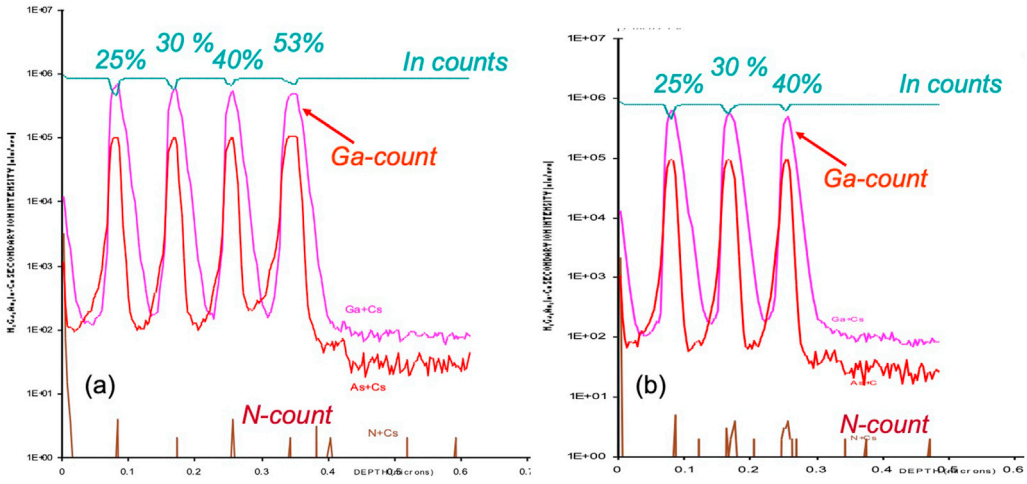

Fig. 26. SIMS measurement of $In_xGa_yAs_{1-y}N_y$ QW layer grown on InP substrates with [DMHy]/V molar ratios of (a) 0.961 and (b) 0.981. The QW host material was grown under tensile-strained state.

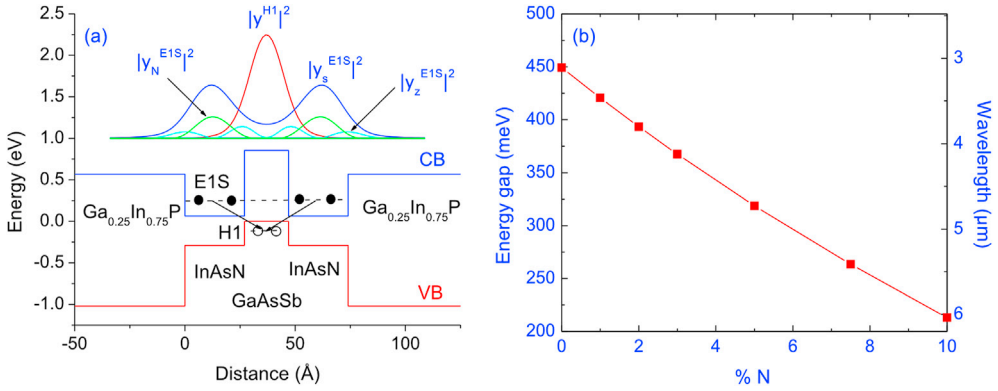

Fig. 27. a) Schematic energy bandgap diagram for the 'W' InAsN-GaAsSb-GaInP Type II QW structure, b) computed emission wavelength as a function of *N*-content. [Adopted from 115].

$GaAs_{0.35}Sb_{0.65}$ (1.2% compressive strain) hole QW is 20 Å thick. The InAsN QWs are in turn surrounded by $In_{0.75}Ga_{0.25}P$ (1.8% tensile strained) barriers (130 Å thick), which provide strain compensation. Since adequate hole confinement often becomes an issue when type-I GaAsN and InGaAsN active regions are employed, the strong confinement of both carrier types here represents an additional advantage of the type-II approach.

For the QW shown in Fig. 27, the calculated optical matrix element, which depends on the square of the electron and hole wavefunction overlap, is approximately 24%, which is similar to that of conventional GaSb-based type II QW structures. The transparency carrier density for the compressively-strained InP-based QW design is similar to that of the GaSb-based type-II QW design, although it exhibits lower gain at the highest carrier densities [115]. Additional gain can be achieved by utilizing a multiple number of stages of the W-structure active region. Detailed studies are needed concerning the strain and layer thicknesses, which could lead to further improvement of the gain characteristics of the InP-based design.

While these design studies project that gain characteristics are comparable to those of GaSb-based type-II QW lasers, the additional advantages of using an InP-substrate-based structure are significant. In general the antimonide processing is more difficult and less mature than InP-based device processing. At 300 K, the thermal conductivity of InP is about twice that of GaSb. Furthermore, compared to InP substrates, GaSb substrates are roughly a factor of three higher in cost, have a 2″-diameter maximum available size, and are of generally inferior quality (i.e. higher defect density). What may be even more relevant, however, is that InP regrowth by MOCVD to bury the heterojunction can substantially improve the thermal management, whereas nothing analogous exists for the antimonides. The proposed structure can utilize InP as the low refractive index cladding layers (*i.e.*, Al-free). GaSb has a high refractive index, so it necessitates the growth of thick AlAsSb cladding layers. The high Al-content layers are undesirable and represent a considerable challenge for adequate facet passivation of reliable high-power lasers.

4.3. Dilute-Bismide QW materials

4.3.1. Dilute-bismide QW lasers

Recently, $GaAs_{1-z}Bi_z$ alloys have drawn much attention due to its rapid reduction in the band gap (E_g) (62–84 meV per Bi mole fraction) with increasing spin-orbit splitting (Δ_{SO}) as Bi concentration increases [191–193]. In particular, suppression in hot hole driven Auger recombination mechanism has been expected to occur when the Bi incorporation exceeds 10%, where Δ_{SO} is larger than E_g. Hot hole driven Auger recombination is a major carrier loss pathway in InP-based telecom wavelength devices, which has been partially responsible for the temperature sensitivity in the threshold current density and slope efficiency. For these reasons, developing $GaAs_{1-z}Bi_z$ based quantum well (QW) active region lasers on GaAs substrates has been a subject of an active research for the last decade, as an alternate to dilute-nitride QWs for achieving lasers emitting in the telecom wavelength regions (λ~1.3–1.55 μm). Such QW active regions are easily incorporated into existing GaAs-based vertical cavity surface emitting laser (VCSEL) architectures employing high-index contrast Distributed Bragg Reflector (DBR) mirrors.

For this reason, significant efforts have been directed towards the pseudomorphic growth of dilute-bismide alloys on GaAs substrates by metalorganic chemical vapor deposition (MOCVD) or molecular beam epitaxy (MBE) in order to realize near-IR emitting devices. Based on the theoretical framework, the origin of the rapid band gap reduction has been attributed to the localized interaction between the Bi resonant level and the valence band of GaAs within a valence band anti-crossing model [191,194]. However, this interaction, taking place in a close proximity with valence band, results in a relatively small conduction band offset at the $GaAs/GaAs_{1-z}Bi_z$ hetero-junction, particularly at low Bi mole fraction. Therefore, the choice of a high bandgap barrier material is of a great importance in order to enhance the electron confinement in the conduction band of the $GaAs_{1-z}Bi_z$ active region.

In addition, the metastable $GaAs_{1-x}Bi_x$ alloy exhibits a large miscibility gap with a very low Bi solubility in GaAs, although it was shown this solubility can be altered in the presence of the strain state [195]. This restriction compels the growth of $GaAs_{1-x}Bi_x$ to be performed with non-typical growth parameters, involving a low growth temperature around 400°*C* and near-stoichiometric V/III flux ratio for MBE and gas-phase ratio for MOCVD, in order to achieve Bi incorporation into the host GaAs matrix [196,197]. In turn, the

growth under the near-stoichiometric condition at such a low temperature can result in point defects and its associated defect complexes, which can act as non-radiative recombination centers within the materials [198]. In addition, particularly for the MOCVD growth, the low growth temperature can lead to high unintentional background carbon contamination as the hydrocarbon radicals from the metal-organic precursors, which are not effectively removed from the growth front, leads to an increased carbon incorporation [197]. This unintentional background carbon has been shown to reduce the minority carrier lifetime [199]. For these reasons, the growth parameters should be carefully optimized for the MOCVD growth of device quality $GaAs_{1-x}Bi_x$ films.

This review focusses on the growth of the $GaAs_{1-z}Bi_z$ QW by MOCVD for device applications, and will address potential pathways to achieve an enhanced Bi incorporation within the QW. In addition, the issues of heterostructure carrier confinement within the Bi-containing active region are discussed based on theoretical and experimental frameworks. The impact of the post-growth thermal annealing on the QW material properties and device performance is detailed. Finally, the characteristics of the laser diodes employing $GaAs_{1-z}Bi_z$ QW active region and recent progress is reviewed.

4.3.2. MOCVD process for $GaAs_{1-z}Bi_z$ QWs

Oe et al. first demonstrated the epitaxial growth of $GaAs_{1-z}Bi_z$ on GaAs substrates by MOCVD, using tri-isopropil-gallium (TIPGa), trimethylbismuth (TMBi), and tertiarybutylarsine (TBAs) at the growth temperature of 365 °C, which is significantly lower than the typical MOCVD growth temperature (~600 °C) employed for GaAs. The TIPGa and TBAs precursors exhibit relatively higher decomposition efficiency at the growth temperature employed. These growth condition resulted in the 0.5 μm-thick $GaAs_{0.976}Bi_{0.024}$ film with the growth rate of 1 μm/h. This 0.5 μm-thick $GaAs_{0.976}Bi_{0.024}$ film has shown a temperature coefficient for the variation in the PL peak position as a function of heat sink temperature as low as 0.1 meV/K, which is significantly smaller than that of GaAs. However, the measured FWHM of the PL spectrum was as large as 60 meV even at 10 K, which can be possibly indicative of significant alloy inhomogeneity and/or disordering.

Further detailed study on the growth of $GaAs_{1-z}Bi_z$ by MOCVD was carried out by Ludewig et al. in 2013 [200]. They have grown $GaAs_{1-z}Bi_z$ multiple quantum wells at varying temperatures with pulsed growth mode, where group III (triethylgallium) and group V precursors (TBAs, TMBi) were supplied in an alternating fashion for 1 s without any pause in between. Notably, the observed that the Bi incorporation levels out as TMBi partial pressure increases, as shown in Fig. 28 (a).

The excess Bi, which was not incorporated during the growth within the "saturated" region, led to the formation of Bi-rich droplets (shown in Fig. 28 (b)). This observation is in contrast to the typical MOCVD process taking place within the mass transport limited regime, where the composition in the solid phase is simply adjusted by varying a partial pressure of precursors in the gas phase. Similar observation of a saturated Bi incorporation as TMBi partial pressure increases was also observed while employing a more conventional continuous flow growth mode where all precursors were simultaneously fed into the reactor [201]. It is worthwhile noting that a significantly low C concentration (as low as $2 \times 10^{16} cm^{-3}$), accompanied with lower growth rates, were obtained from a sample grown within the Bi saturation region, which was explained by the segregated Bi atoms blocking the C incorporation sites. GaAs grown within the similar growth condition typically exhibits the C concentration on the order of $\sim 10^{20} cm^{-3}$ [198]. The growth rate reduction at a high TMBi partial pressure was further elucidated by Forghani et al., which was ascribed to site blocking through the formation of a methyl-terminated surface, wherein the methyl groups are attached to surface Bi atoms [202]. This finding suggests that an optimized

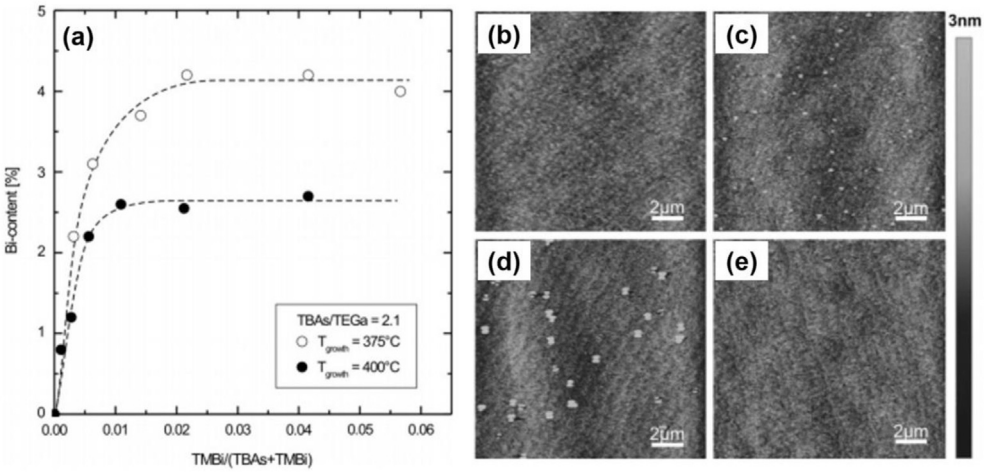

Fig. 28. (a) Bi fraction depending on the TMBi partial pressure for samples grown at 375 °C and 400 °C. If the temperature is only reduced by 25 °C the Bi fraction can be raised from 2.7% to 4.2%. The dashed lines are again only guides to the eye. (b–e) Surface morphology of the Ga(AsBi)/GaAs MQWs depending on the TMBi partial pressure and the growth temperature. (b)–(d) were grown at a temperature of 400 °C with TMBi/V ratios of (b) 0.0056; (c) 0.021 and (d) 0.042. (e) was grown at a reduced temperature of 375 °C. For low TMBi/V ratio smooth surfaces with no droplet formation were observed. If the TMBi partial pressure is increased Bi droplets occur. For the low temperature growth with a Bi concentration of 4.2% also droplet free surfaces were realized. (Adopted from reference 200).

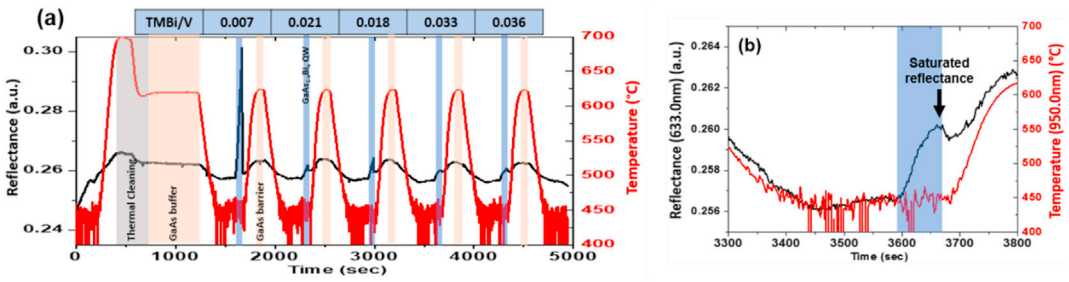

Fig. 29. (a) *in situ* reflectance measured during the growth of $GaAs_{1-z}Bi_z$ MQW structure with varying TMBi/V ratio, and (b) *in situ* reflectance measured during the growth of $GaAs_{1-z}Bi_z$ QW at TMBi/V ratio of 0.033.

growth condition can lead to a significantly lower background carbon concentration during the growth of $GaAs_{1-z}Bi_z$ thin film growth by MOCVD, and the simultaneous growth rate reduction can be observed as a result of the surface blocking effect.

Similarly, a relatively low C incorporation, $\sim 5 \times 10^{17} cm^{-3}$, was also observed by Kim et al. from a $GaAs_{0.965}Bi_{0.035}$ MQW structure grown by a continuous growth mode [203] where an *in situ* reflectance measurement (shown in Fig. 29(a) and (b)) was utilized to find the growth conditions at which the Bi incorporation saturates, by observing the onset of a growth rate reduction. However, a graded Bi profile within the $GaAs_{1-z}Bi_z$, investigated by STEM measurements, have remained as an issue yet to be solved when the $GaAs_{1-z}Bi_z$ growth takes place within the Bi saturated regime under the continuous growth mode [204].

4.3.3. Recent progress of electrically injected $GaAs_{1-z}Bi_z$ QW lasers grown by MOCVD

Driven by the potential advantages of $GaAs_{1-z}Bi_z$, which include a low temperature sensitivity in the emission wavelength and expected higher wall plug efficiency by the suppressed Auger related carrier loss, optically/electrically pumped $GaAs_{1-z}Bi_z$ QW lasers have been demonstrated by several research groups to date [205–213]. The first demonstration of electrically injected $GaAs_{1-z}Bi_z$ QW laser was realized by Ludewig et al. [205]. The laser heterostructure consists of a $GaAs_{0.978}Bi_{0.022}$ single QW (7 nm thick) active region, which was grown by a pulsed growth mode described in the previous section, sandwiched by $Al_{0.2}Ga_{0.8}As$ waveguide layers and $Al_{0.4}Ga_{0.6}As$ cladding layers. By photoluminescence study, this work showed an enhanced luminescence efficiency when an $Al_{0.2}Ga_{0.8}As$ barrier was employed in comparison to that with GaAs barrier, which was ascribed to an improved carrier confinement and an annealing effect during the growth of the $Al_yGa_{1-y}As$ at higher temperature.

In a follow-up study, further reduction in the J_{th} (1–1.1 kA/cm^2) was reported by Marko et al. from a structure, which employs $Al_{0.12}Ga_{0.88}As$ waveguide layers but with same $GaAs_{0.978}Bi_{0.022}$ single QW active region [206], which is consistent with the increase in the optical confinement factor (Γ~0.89% ($Al_{0.2}Ga_{0.8}As$ waveguide layer) vs. Γ~1.21% ($Al_{0.12}Ga_{0.88}As$ waveguide layer)). It must be noted that a non-pinned carrier density above threshold was observed from these $GaAs_{0.978}Bi_{0.022}$ SQW lasers [206], in contrast to an ideal diode laser, where the carrier density pins above threshold due to the fast stimulated emission process and the subsequent pinning of the quasi-Fermi level. The observed carrier non-pinning was explained by the defect-related recombination dominating the device performance.

Later, Kim et al. also demonstrated MOCVD grown $GaAs_{1-z}Bi_z$ QW lasers with GaBi mole fraction ranging from 2.5 to 3.5%, by using continuous flow MOCVD process and with $GaAs_{1-y}P_y$ tensile strained barrier [204,212,213]. With post growth thermal annealing, a reduced threshold current density (5.9 vs. 4.1 kA/cm^2) at room temperature for a $GaAs_{0.975}Bi_{0.025}/GaAs_{0.8}P_{0.2}$ QW active region laser with the lasing wavelength near 960–962 nm was observed, which was ascribed to the reduction in the point defects through thermal annealing. In addition, devices with a GaAs barrier structure show excessive carrier band-filling and thermionic leakage at room temperature associated with a low conduction band offset, resulting in lasing emission at a higher transition energy. A more detailed investigation on the effect of post-growth thermal annealing was carried out in follow-up studies, using a $GaAs_{0.965}Bi_{0.035}$/-GaAs/$GaAs_{0.75}P_{0.25}$ (5/1/5 nm) QW active region laser [204,213]. These studies have shown a gradual decrease in the laser slope efficiency as the annealing time increases, while the maximum PL intensity, as well as the lowest J_{th} (~5.3 kA/cm^2), were obtained when annealed for 30 min at 630 °C, demonstrating that there exists an optimum window for the post growth thermal annealing. This observation was further investigated by cavity length analysis, with evidence of a minimal degree of carrier nonpinining, by Kim et al. [213]. They showed degraded internal differential quantum efficiencies with increasing annealing time while the change in the extracted peak modal gain follows the same trend as the variation in the photoluminescence intensity [213].

Recently, room temperature operation of a MBE grown $GaAs_{0.942}Bi_{0.058}$ SQW diode laser has been reported, which emits at a wavelength of 1142 nm with the threshold current density of 3.89 kA/cm^2 [214] (see Fig. 30). This result represents the longest emission wavelength from SQW $GaAs_{1-z}Bi_z$ lasers reported up to date. By contrast, MOCVD-grown $GaAs_{1-z}Bi_z$ SQW lasers have reported lasing as long as 1039 nm (from $GaAs_{0.956}Bi_{0.044}$ SQW active region at the maximum operating temperature of 180 K) [205]. Therefore, it is necessary to understand the pathways for achieving higher incorporation of Bi within the $GaAs_{1-z}Bi_z$ QW active region by the MOCVD process, while maintaining good luminescent properties, in order to achieve both the emission wavelength closer to telecom O band (~1.3 μm) and the expected higher wall-plug efficiency by the suppression of hot hole driven Auger recombination.

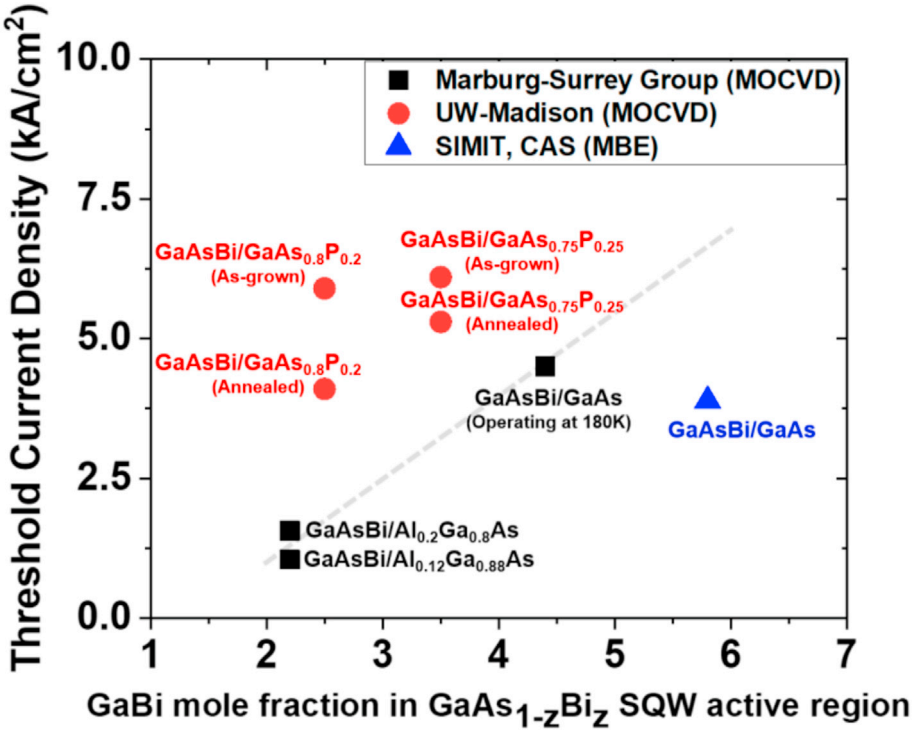

Fig. 30. The reported threshold current density for GaAsBi SQW based lasers operating at room temperature where the results of Marburg-Surrey group are from reference 206, those of UW-Madison are from reference 204, 212, and that of SIMIT, CAS is from reference 214.

4.3.4. Outlook for higher Bi-content $GaAs_{1-z}Bi_z$ active region

Within the kinetic limited regime during the MOCVD process, various parameters in the growth condition can affect the process in the incorporation of Bi during the $GaAs_{1-z}Bi_z$ growth, which includes growth temperature, V/III partial pressure ratio, TMBi/V ratio, growth sequences, growth pressure and surface steps. One common observation is the increase in the Bi incorporation by the reduction in growth temperature. As shown in Fig. 28, Ludewig et al. has observed the increase in the Bi concentration from 2.2 to 4.2% by reducing the growth temperature by 25 °C [200]. Similar observations were made by Kim et al. where reduced GaBi mole fractions (2.6, 3,4, and 4.3%) were obtained when higher growth temperatures were employed (400, 420, and 440 °C) [212]. It is noteworthy that the materials grown at lower temperature exhibited a significantly lower luminescent efficiency, as evident from PL measurements, which was attributed to various types of non-radiative defects associated with Bi-related defects and other point defects originating from the lower growth temperature. Nevertheless, with a lower growth temperature and relatively low V/III partial pressure ratio, Ludewig et al. have demonstrated the Bi incorporation in excess of 7% of GaBi mole fraction on (001) GaAs substrate [201], although more detailed optical/structural characterizations are necessary to further understand the nature of defects originating from the low temperature growth.

The use of a high index plane (311) GaAs substrate may also offer a pathway for enhancing Bi incorporation within the $GaAs_{1-z}Bi_z$ QW active region, while mitigating the need for very low growth temperatures. The GaAs (311) surface exhibits (100) terraces and (111) step-edge atoms. For the (311)B plane, (100)-like Ga atoms and (111)B-like As atoms are present on the surface. As a result, (311)B substrates have been employed to obtain the desired structural/optical properties within the epitaxial layer such as an improved InAs QD areal density [215], a higher N incorporation within GaAsN film [216], and enhanced incorporation of Bi within the bulk $GaAs_{1-z}Bi_z$ film on (311)B GaAs substrate by MBE [217]. For the $GaAs_{1-z}Bi_z$ growth by MOCVD, initial studies indicates that a higher Bi incorporation within a $GaAs_{1-z}Bi_z$ QW on (311)B GaAs substrate can be obtained.

From HR-XRD measurements, a higher GaBi mole fraction (z = 6.4%) within the $GaAs_{1-z}Bi_z$ MQW was identified as a result of using (311)B GaAs substrate, in comparison to z = 2.6% grown on (001) GaAs substrate, while these materials were simultaneously grown at 440 °C under the same condition (Table 1) [218]. This higher Bi incorporation is evident from the PL spectra taken at room temperature, as shown in Fig. 31. The sample grown on a (311)B GaAs substrate exhibits the PL peak position of 1145 nm, or equivalently 1.083eV, while that grown on (001) shows the PL peak position of 980 nm (1.265eV). The inset figure shows the PL spectra from 5-period $GaAs_{0.936}Bi_{0.064}$/GaAs MQW sample, grown on (311)B GaAs substrate, taken before and after *in situ* annealing under AsH_3/H_2 ambient at 630 °C for 30 min. 7-fold increase in the PL intensity was observed after the post-growth *in situ* annealing, indicating a substantial increase in the radiative efficiency of the $GaAs_{0.936}Bi_{0.064}$ QWs. However, the FWHM in the PL linewidth was as broad as 189 meV, which is significantly larger than the 95 meV value observed from the $GaAs_{0.974}Bi_{0.026}$ QWs grown on (001) GaAs. This broader

Table 1
Structure Details and $GaAs_{1-z}Bi_z$ growth rate on a different crystallographic plane.

Crystallographic Plane	Structure Details from the HR-XRD dynamic simulation	$GaAs_{1-z}Bi_z$ Growth Rate [nm/sec]	PL Peak Position [eV]
(001)	5× GaAs0.974Bi0.026/GaAs (8/23 m)	0.089	1.265
(311)B	**5x $GaAs_{0.936}Bi_{0.064}$/GaAs (10.5/30 nm)**	**0.117**	**1.083**

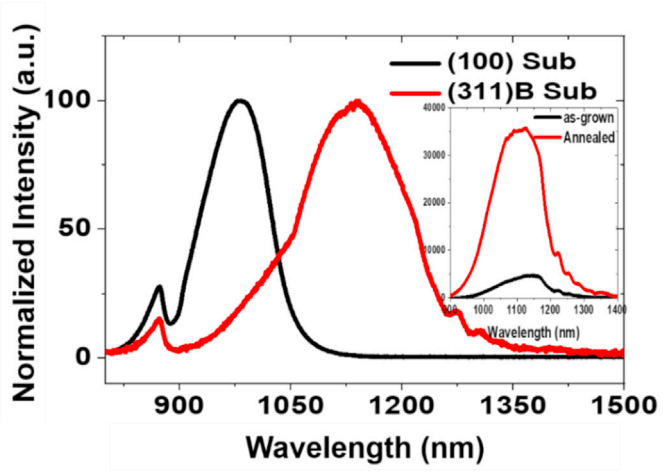

Fig. 31. Normalized PL spectra taken from as-grown 5× $GaAs_{1-z}Bi_z$. MQWs grown on either (100) or (311)B GaAs substrate where a clear redshift in the mission wavelength peak position is observed from the MQW sample grown on (311)B substrate. Inset shows the PL spectra taken before and after the post-growth thermal annealing for the MQW grown on a (311)B substrate.

FWHM potentially indicates the presence of nonhomogeneous Bi distribution and/or abundant localized states. Therefore, further improvements for reducing the emission linewidth is necessary.

Another approach to increase the emission wavelength is to employ a type-II quantum well heterostructure, by which electrons and holes can recombine by a diagonal transition in a close proximity, as shown in Fig. 32(a). $GaAs_{1-z}Bi_z$ exhibits a large valence band offset (~55 meV), in comparison to the that of $GaAs_{1-y}Sb_y$ [219], which is the conventional approach used for the type II QW heterostructure. $GaAs_{1-z}Bi_z$ is also advantageous because it possesses a smaller compressive strain on GaAs, compared with $GaAs_{1-y}Sb_y$ for similar band offsets. Therefore, research efforts have been directed to demonstrate $GaAs_{1-z}Bi_z$ based type-II heterostructure by either MBE or MOCVD process [118,218,220,221].

$GaAs_{1-z}Bi_z/In_yGa_{1-y}As$ type-II heterostructures were first demonstrated by the MBE process [118] where Li et al. has shown an extended emission wavelength up to 1230 nm at room temperature (Fig. 32(b)) by using $In_{0.18}Ga_{0.82}As/GaAs_{0.966}Bi_{0.034}$ type-II heterostructure. Later, Kim et al. also shown an extended wavelength up to 1.17 μm at room temperature by using a

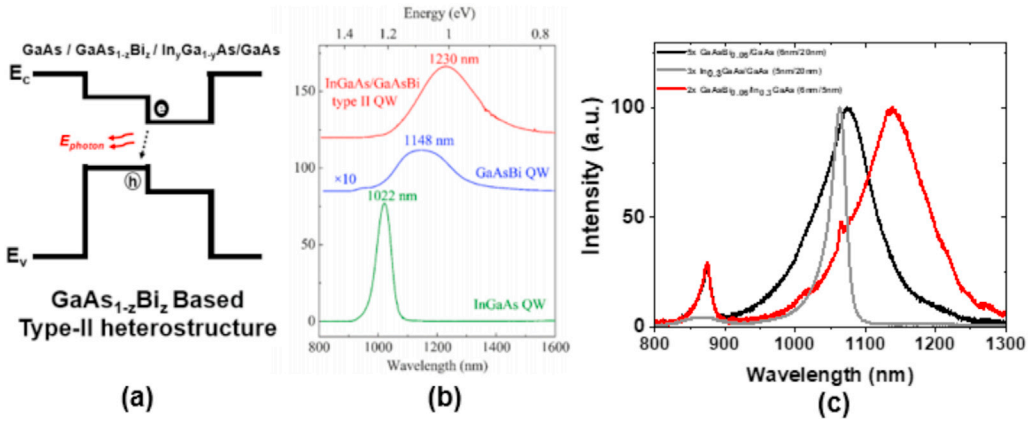

Fig. 32. (a) Schematic band diagram of $GaAs_{1-z}Bi_z/In_yGa_{1-y}As$ type-II heterostructure, (b). Room temperature PL of $In_{0.18}Ga_{0.82}As/GaAs_{0.966}Bi_{0.034}$, GaAsBi/GaAs and $In_{0.18}Ga_{0.82}As$/GaAs single QWs from by MBE (Adopted from reference 30), and (c) Normalized photoluminescence spectra from 5-period $GaAs_{0.94}Bi_{0.06}$/GaAs MQW, 3-period $In_{0.3}Ga_{0.7}As$ MQW, and 2-period $GaAs_{0.94}Bi_{0.06}/In_{0.3}Ga_{0.7}As$/GaAs MQW structure grown by MOCVD (Adopted from reference 218).

$GaAs_{0.94}Bi_{0.06}/In_{0.3}Ga_{0.7}As$ heterostructure grown by the MOCVD process (Fig. 32(c)) [218]. In addition, Broderick et al. used an $GaAs_{1-y}N_y$ electron well, instead of InGaAs, which takes advantage of both the large conduction band offset of $GaAs_{1-y}N_y$ and a large valence band offset from employing $GaAs_{1-z}Bi_z$. This work demonstrated a further extended emission wavelength up to 1.72 μm, although improving luminescent properties remain as a subject of future study [221]. Furthermore, demonstration of $GaAs_{1-z}Bi_z/In_{y-}Ga_{1-y}As(N)$ type-II heterostructures as a laser active region is yet to be realized, which can be further explored by employing "W-type" heterostructure in order to increase electron-hole wavefunction overlap [98].

5. Conclusions

Strained-QW active regions have made a tremendous impact on the performance of diode lasers. The ternary InGaAs material system has proven most successful for accessing near-infrared emission wavelengths from $\lambda \sim 0.87$–1.2 μm. Such devices have demonstrated the highest total power conversion efficiencies for any type of laser. While highest performance and reliability has been realized for wavelengths $\lambda < 1$ μm, challenges remain for long term reliability at longer emission wavelengths.

Metastable QW materials provide a pathway to extend emission wavelengths well beyond the strain limitations imposed for the growth of InGaAs QWs on GaAs substrates. Examples of such materials are InGaAsP on GaAs, dilute-nitride InGaAsN, and dilute-bismide GaAsBi compounds. MOCVD growth conditions have been established to kinetically inhibit strain relaxation and compositional phase separation, as well as increase the anion incorporation efficiency in these alloys. While device performance is still largely limited by the structure uniformity and radiative properties of these metastable materials, theoretical projections point towards the potential for dramatic performance improvements over conventional QW based devices. There does not appear to be any fundamental limitations for the application of these metastable materials to realize high performance devices, rather the remaining challenges are believed to originate from finding the appropriate MOCVD growth processes to reduce defect recombination (i.e. improve radiative efficiency), increase anion solubility, and improve structural uniformity. Futhermore, there is generally a lack of studies to establish long term laser reliability for devices employing the highly metastable materials.

Acknowledgement

The work at UW-Madison was partially supported by the National Science Foundation (ECCS 180628), and Army Research Office (ARO W911NF2010185). The work at Lehigh University was partially supported by the US National Science Foundation (ECCS 1408051 and DMR 1505122) and the Daniel E. '39 and Patricia M. Smith Endowed Chair Professorship Fund.

References

[1] P. Urquhart, Review of rare earth doped fiber lasers and amplifiers, IEE Proc. J (Optoelectronics) 135 (1988) 385–407.
[2] W.T. Tsang, Extremely low threshold (AlGa)As graded-index waveguide separate-confinement heterostructure lasers grown by molecular-beam epitaxy, Appl. Phys. Lett. 40 (1982) 217–219.
[3] R.D. Dupuis, III-V semiconductor heterojunction devices grown by metalorganic chemical vapor deposition, IEEE J. Sel. Top. Quant. Electron. 6 (2000) 1040–1050.
[4] J.W. Matthews, A.E. Blakeslee, Defects in epitaxial multilayers: I. Misfit dislocations, J. Cryst. Growth 27 (1974) 118–125.
[5] M.D. Camras, J.M. Brown, N. Holonyak Jr., M.A. Nixon, R.W. Kaliski, M.J. Ludowise, W.T. Dietze, C.R. Lewis, Stimulated emission in strained-layer quantum-well heterostructures, J. Appl. Phys. 54 (1983) 6183–6189.
[6] M.J. Ludowise, W.T. Dietze, C.R. Lewis, M.D. Camras, N. Holonyak Jr., B.K. Fuller, M.A. Nixon, Continuous 300-K laser operation of strained superlattices, Appl. Phys. Lett. 42 (1983) 487–489.
[7] W.D. Laidig, P.J. Caldwell, Y.F. Lin, C.K. Peng, Strained-layer quantum-well injection laser, Appl. Phys. Lett. 44 (1984) 653–655.
[8] W.D. Laidig, Y.F. Lin, P.J. Caldwell, Properties of InxGa1-xAs-GaAs strained-layer quantum-well-heterostructure injection lasers, J. Appl. Phys. 57 (1985) 33–38.
[9] C. Lauer, H. Konig, G. Gronninger, S. Hein, A. Gomez-Iglesias, M. Furitsch, J. Maric, H. Kissel, P. Wolf, J. Biesenbach, U. Straub, Advances in performance and beam quality of 9xx nm laser diodes tailored for efficient fiber coupling, in: Proc. SPIE 8241, High-Power Diode Laser Technology and Applications X, 2012, p. 824111.
[10] G.M. Smith, J.J. Coleman, Quantum well heterostructure lasers, in: N.G. Einspruch, W.R. Frensley (Eds.), Heterostructures and Quantum Devices, Academic Press, San Diego, 1994, pp. 215–241.
[11] G.H. Olsen, C.J. Nuese, R.T. Smith, The effect of elastic strain on energy bandgap and lattice parameter in III-V compounds, J. Appl. Phys. 49 (1978) 5523–5529.
[12] N.G. Anderson, W.D. Laidig, R.M. Kolbas, Y.C. Lo, Optical characterization of pseudomorphic InxGa1-xAs-GaAs single-quantum-well heterostructures, J. Appl. Phys. 60 (1986) 2361–2367.
[13] J.E. Schirber, I.J. Fritz, L.R. Dawson, Light-hole conduction in InGaAs/GaAs strained-layer superlattices, Appl. Phys. Lett. 46 (1985) 187–189.
[14] E.P. O'Reilly, Valence band engineering in strained-layer structures, Semicond. Sci. Technol. 4 (1989) 121–137.
[15] B.K. Ridley, The in-plane effective mass in strained-layer quantum wells, J. Appl. Phys. 68 (1990) 4667–4673.
[16] E. Yablonovitch, E.O. Kane, Reduction of lasing threshold current density by the lowering of valence band effective mass, J. Lightwave Technol. 4 (1986) 504–506.
[17] E. Yablonovitch, E.O. Kane, Band structure engineering of semiconductor lasers for optical communications, J. Lightwave Technol. 6 (1988) 1292–1299.
[18] A.R. Adams, Band-structure engineering for low-threshold high-efficiency semiconductor lasers, Electron. Lett. 22 (1986) 249–250.
[19] K.J. Beernink, P.K. York, J.J. Coleman, Dependence of threshold current density on quantum well composition for strained-layer InGaAs-GaAs lasers by metalorganic chemical vapor deposition, Appl. Phys. Lett. 55 (1989) 2585–2587.
[20] K.J. Beernink, P.K. York, J.J. Coleman, R.G. Waters, J. Kim, C.M. Wayman, Characterization of InGaAs-GaAs strained-layer lasers with quantum wells near the critical thickness, Appl. Phys. Lett. 55 (1989) 2167–2169.
[21] R.G. Waters, R.K. Bertaska, Dark-line observations in failed quantum well lasers, Appl. Phys. Lett. 52 (1988) 1347–1348.
[22] R.G. Waters, D.P. Bour, S.L. Yellen, N.F. Ruggieri, Inhibited dark-line defect formation in Strained InGaAs/AlGaAs quantum well lasers, IEEE Photon. Technol. Lett. 2 (1990) 531–533.
[23] K. Fukagai, S. Ishikawa, K. Endo, T. Yuasa, Current density dependence for dark-line defect growth velocity in strained InGaAs/AlGaAs quantum well laser diodes, Jpn. J. Appl. Phys. 30 (1991) L371–L373.

[24] A. Moser, A. Oosenbrug, E.E. Latta, T. Forster, M. Gasser, High-power operation of strained InGaAs/AlGaAs single quantum well lasers, Appl. Phys. Lett. 59 (1991) 2642–2644.
[25] P.K. York, K.J. Beernink, G.E. Fernandez, J.J. Coleman, InGaAs-GaAs-AlGaAs strained-layer quantum well lasers by metal-organic chemical vapour deposition, Semicond. Sci. Technol. 5 (1990) 508–511.
[26] F.A. Houle, D.L. Neiman, W.C. Tang, H.J. Rosen, Chemical changes accompanying facet degradation of AlGaAs quantum well lasers, J. Appl. Phys. 72 (1992) 3884–3896.
[27] M. Gasser, and E. E. Latta, Method of Mirror Passivation of Semiconductor Laser Diodes, U.S. Patent No. 5665637, 1991..
[28] L.W. Tu, E.F. Schubert, M. Hong, G.J. Zydzik, In-vacuum cleaving and coating of semiconductor laser facets using thin silicon and a dielectric, J. Appl. Phys. 80 (1996) 6448–6451.
[29] H. Horie, H. Ohta, T. Fujimori, Reliability improvement of 980-nm laser diodes with a new facet passivation process, IEEE J. Sel. Top. Quant. Electron. 5 (1999) 832–838.
[30] P. Ressel, G. Erbert, U. Zeimer, K. Hausler, G. Beister, B. Sumpf, A. Klehr, G. Trankle, Novel passivation process for the mirror facets of Al-free active region high-power semiconductor diode lasers, IEEE Photon. Technol. Lett. 17 (2005) 962–964.
[31] G. M. Smith, D. A. S. Loeber, and S. D. Solimine, High power 980 nm pump lasers, in LEOS 2000 - IEEE Lasers and Electro-Optics Society 13th Annual Meeting Conference Proceedings.
[32] G.M. Smith, G. Yang, M. K. Davis, S. D. Solimine, R. Bhat, W. Liu, D. A. S. Loeber, F. Yang, A. Kussmaul, M. H. Hu, X. S. Liu, and C. E. Zah, Design, performance, and reliability of 980 nm pump lasers, in LEOS 2003 - IEEE Lasers and Electro-Optics Society 16th Annual Meeting Conference Proceedings.
[33] G. Yang, G.M. Smith, M.K. Davis, D.A.S. Loeber, M. Hu, C.E. Zah, R. Bhat, Highly reliable high-power 980-nm pump laser, Photon. Technol. Lett. 16 (No. 11) (2004) 2403–2405.
[34] G. Yang, G.M. Smith, M.K. Davis, A. Kussmaul, D.A.S. Loeber, M. Hu, H.K. Nguyen, C.E. Zah, R. Bhat, High-performance 980-nm ridge waveguide laser with a nearly circular beam, IEEE Photon. Technol. Lett. 16 (2004) 981–983.
[35] R.L. Thornton, D.F. Welch, R.D. Burnham, T.L. Paoli, P.S. Cross, High power (2.1 W) 10-stripe AlGaAs laser arrays with Si disordered facet windows, Appl. Phys. Lett. 49 (1986) 1572–1574.
[36] R.M. Lammert, S.W. Oh, M.L. Osowski, C. Panja, P. T Rudy, T. Stakelon, J.E. Ungar, Advances in high brightness high power semiconductor lasers, in: Proc. SPIE 6216, Laser Source and System Technology for Defense and Security II, 2006, p. 62160B.
[37] S. Balsamo, G. Ghislotti, F. Trezzi, P. Bravetti, G. Coli, S. Morasca, High-power 980-nm pump lasers with flared waveguide design, J. Lightwave Technol. 20 (2002) 1512–1516.
[38] M.A. Bettiati, C. Starck, F. Laruelle, V. Cargemel, P. Pagnod, P. Garabedian, D. Keller, G. Ughetto, J.C. Bertreux, L. Raymond, G. Gelly, R.M. Capella, Very high power operation of 980-nm single-mode InGaAs/AlGaAs pump lasers, Proc. SPIE 6104, High-Power Diode Laser Technology and Applications IV (2006) 61040F.
[39] N. Moshegov, I. Berezin, A. Komissarov, P. Trubenko, D. Miftakhutdinov, I. Bereshev, V. Chuyanov, N. Strougov, A. Ovtchinnikov, V. Gapontsev, Highly-efficient high-power pumps for QCW fiber lasers, Proc. SPIE 10900, High-Power Diode Laser Technology XVII (2019) 109000G.
[40] C.M. Stickley, M.E. Filipkowski, E. Parra, E.E. Hach III, Overview of progress in super high efficiency diodes for pumping high energy lasers, Proc. SPIE 6104, High-Power Diode Laser Technology and Applications IV (2006) 610405.
[41] P. Crump, W. Dong, M. Grimshaw, J. Wang, S. Patterson, D. Wise, M. DeFranza, S. Elim, S. Zhang, M. Bougher, J. Patterson, S. Das, J. Bell, J. Farmer, M. DeVito, R. Martinsen, 100-W+ diode laser bars show > 71% power conversion from 790- to 1000-nm and have clear route to >85%, Proc. SPIE 6456, High-Power Diode Laser Technology and Applications V (2007) 64560M.
[42] M. Peters, V. Rossin, B. Acklin, High-efficiency, high-reliability laser diodes at JDS Uniphase, Proc. SPIE 5711, High-Power Diode Laser Technology and Applications III (2005) 142–151.
[43] M. Kanskar, T. Earles, T.J. Goodnough, E. Stiers, D. Botez, L.J. Mawst, 73% CW power conversion efficiency at 50 W from 970 nm diode laser bars, Electron. Lett. 41 (2005) 245–247.
[44] S.-S. Schad, T. Gottwald, V. Kuhn, M. Ackermann, D. Bauer, M. Scharun, A. Killi, Recent development of disk lasers at TRUMPF, Proc. SPIE 9726, Solid State Lasers XXV (2016) 972615.
[45] S.J. Freedberg Jr., Star Wars at Sea: Navy's Laser Gets Real, BreakingDefense.com, 2014.
[46] J.R. Wilson, Laser weapons get ready for the big time, Mil. Aero. Electron. 31 (2020) 12–19.
[47] J.G. Bai, P. Leisher, S. Zhang, S. Elim, M. Grimshaw, C. Bai, L. Bintz, D. Dawson, L. Bao, J. Wang, M. DeVito, R. Martinsen, J. Haden, Mitigation of thermal lensing effect as a brightness limitation of high-power broad area diode lasers, Proc. SPIE 7953, Novel In-Plane Semiconductor Lasers X (2011) 79531F.
[48] P. Crump, S. Boldicke, C.M. Schultz, H. Ekhteraei, H. Wenzel, G. Ebert, Experimental and theoretical analysis of the dominant lateral waveguiding mechanism in 975 nm high power broad area laser diodes, Semicond. Sci. Technol. 25 (2012), 045001.
[49] M. Kanskar, C. Bai, L. Bao, Z. Chen, C. Chiong, M. DeFranza, K. Fortier, M. Hemenway, S. Li, E. Martin, J. Small, B. Tomakian, W. Urbanek, B. Wilkins, J. Zhang, High brightness diodes and 600 W 62% efficient low SWAP fiber-coupled package, Proc. SPIE 11262, High-Power Diode Laser Technology and Applications XVIII (2020) 112620A.
[50] A. Bachmann, C. Lauer, M. Furitsch, H. Konig, M. Muller, U. Straub, Recent brightness improvements of 976 nm high power laser bars, Proc. SPIE 10086, High-Power Diode Laser Technology and Applications XV (2017) 1008602.
[51] C. Ebert, T. Guiney, J. Braker, D. Stapleton, K. Alegria, D. Irwin, Advances in the power, brightness, weight and efficiency of fiber-coupled diode lasers for pumping and direct diode applications, Proc. SPIE 10086, High-Power Diode Laser Technology and Applications XV (2017) 1008607.
[52] V. Gapontsev, N. Moshegov, I. Berezin, A. Komissarov, P. Trubenko, D. Miftakhutdinov, I. Berishev, V. Chuyanov, O. Raisky, A. Ovtchinnikov, Highly-efficient high-power pumps for fiber lasers, Proc. SPIE 10086, High-Power Diode Laser Technology and Applications XV (2017) 1008604.
[53] J. Skidmore, M. Peters, V. Rossin, J. Guo, Y. Xiao, J. Cheng, A. Shieh, R. Srinivasan, J. Singh, C. Wei, R. Duesterberg, E. Zucker, Advances in high-power 9xxnm laser diodes for pumping fiber lasers, Proc. SPIE 9733, High-Power Diode Laser Technology and Applications XIV (2016) 97330B.
[54] N. Bandyopadhyay, Y. Bai, B. Gokden, A. Myzaferi, S. Tsao, S. Slivken, M. Razeghi, Watt level performance of quantum cascade lasers in room temperature continuous wave operation at λ∼3.76μm, Appl. Phys. Lett. 97 (2010) 131117.
[55] M. Mitsuhara, M. Ogasawara, M. Oishi, H. Sugiura, K. Kasaya, 2.05-μm wavelength InGaAs-InGaAs distributed-feedback multiquantum-well lasers with 10-mW output power, IEEE Photon. Technol. Lett. 11 (1999) 33–35.
[56] T. Sato, K. Mitsuhara, T. Watanabe, K. Kasaya, T. Takeshita, Y. Kondo, 2.1-μm-Wavelength InGaAs multiple-quantum-well distributed feedback lasers grown by MOVPE using Sb surfactant, IEEE J. Sel. Top. Quant. Electron. 13 (2007) 1079–1083.
[57] T. Sato, M. Mitsuhara, T. Watanabe, Y. Kondo, Surfactant-mediated growth of InGaAs multiple-quantum-well lasers emitting at 2.1 μm by metalorganic vapor phase epitaxy, Appl. Phys. Lett. 87 (2005) 211903.
[58] T. Sato, M. Mitsuhara, Y. Kondo, 2.33 μm-wavelength InAs/InGaAs multiple-quantum-well lasers grown by MOVPE, Electron. Lett. 43 (2007) 1143–1145.
[59] T. Sato, M. Mitsuhara, N. Nunoya, T. Fujisawa, K. Kasaya, F. Kano, Y. Kondo, 2.33-μm-Wavelength distributed feedback lasers with InAs/InGaAs multiple-quantum wells on InP substrates, IEEE Photon. Technol. Lett. 20 (2008) 1045–1047.
[60] T. Sato, M. Mitsuhara, T. Kakitsuka, T. Fujisawa, Y. Kondo, Metalorganic vapor phase epitaxial growth of InAs/InGaAs multiple quantum well structures on InP substrates, IEEE J. Sel. Top. Quant. Electron. 14 (2008) 992–997.
[61] S. Kim, J. Kirch, L. Mawst, Highly-Strained InAs quantum wells on InP substrates for mid-IR emission, J. Cryst. Growth 312 (2010) 1388–1390.
[62] D.P. Bour, Ramon U. Martinelli, D.B. Gilbert, L. Elbaum, M.G. Harvey, Operating characteristics of InGaAs/AlGaAs strained single quantum well lasers, Appl. Phys. Lett. 55 (1989) 1501.
[63] W.-J. Choi, P.D. Dapkus, J.J. Jewell, 1.2-μm GaAsP/InGaAs strain compensated single-quantum-well diode laser on GaAs using metal-organic chemical vapor deposition, IEEE Photon. Technol. Lett. 11 (1999) 1572–1574.
[64] D. Schlenker, T. Miyamoto, Z. Chen, F. Koyama, K. Iga, Ext. Abstr, in: 59th Autumn Meet, Japan Society of Applied Physics, 1998, p. 18. YA-6.

[65] D. Schlenker, T. Miyamoto, Z.B. Chen, M. Kawaguchi, T. Kondo, E. Gouardes, F. Koyama, K. Iga, Critical layer thickness of 1.2-μm highly strained GaInAs/GaAs quantum wells, J. Cryst. Growth 221 (2000) 503–508.
[66] F. Bugge, R. Bege, G. Blume, D. Feise, B. Sumpf, N. Werner, U. Zeimer, K. Paschke, M. Weyers, Lifetime behavior of laser diodes with highly strained InGaAs QWs and emission wavelength between 1120 nm and 1180 nm, J. Cryst. Growth 491 (2018) 31–35.
[67] J.J. Coleman, Strained-layer InGaAs quantum-well heterostructure lasers, IEEE J. Sel. Top. Quant. Electron. 6 (2000) 1008–1013.
[68] J.Y. Tsao, Coherency and semi-coherency, in: Materials Fundamentals of Molecular Beam Epitaxy, Academic, Boston, 1993, pp. 183–186.
[69] S. Sato, S. Satoh, 1.21 μm continuous-wave operation of highly strained GaInAs quantum well lasers on GaAs substrates, Jpn. J. Appl. Phys. 38 (1999) L990–L992.
[70] F. Koyama, D. Schlenker, T. Miyamoto T, Z. Chen, A. Matsutani, T. Sakaguchi, K. Iga, 1.2 μm highly strained GaInAs/GaAs quantum well lasers for single mode fiber datalink, Electron. Lett. 35 (1999) 1079–1081.
[71] K. Kim, Y.H. Lee, Temperature-dependent critical thickness for strained-layer heterostructures, Appl. Phys. Lett. 67 (1995) 2212–2214.
[72] M.J. Ekenstedt, S.M. Wang, T.G. Andersson, Temperature-dependent critical layer thickness for $In_{0.36}Ga_{0.64}As$/GaAs single quantum wells, Appl. Phys. Lett. 58 (1991) 854–855.
[73] J.W. Matthews, A.E. Blakeslee, Defects in epitaxial multilayers: I. Misfit dislocations, J. Cryst. Growth 27 (1974) 118–125.
[74] N. Tansu, L.J. Mawst, High-performance strain compensated InGaAs-GaAsP-GaAs ($\lambda = 1.17$ μm) quantum well diode lasers, IEEE Photon. Technol. Lett. 13 (2001) 179–181.
[75] N. Tansu, J.Y. Yeh, L.J. Mawst, Physics and characteristics of high performance 1200nm InGaAs and 1300-1400 nm InGaAsN QW lasers obtained by MOCVD, J. Phys. Condens. Matter 16 (2004) S3277.
[76] W. Sun, H. Kim, L.J. Mawst, N. Tansu, Interplay of GaAsP barrier and strain compensation in InGaAs quantum well at near-critical thickness, J. Cryst. Growth 531 (2020) 125381.
[77] R. People, J.C. Bean, Calculation of critical layer thickness versus lattice mismatch for Ge_xSi_{1-x}/Si strained-layer heterostructures, Appl. Phys. Lett. 47 (1985) 322.
[78] V.D. Jovanovic, Strained quantum wells, in: P. Harrison A, Valavanis (Eds.), Quantum Wells, Wires and Dots, Wiley, Hoboken, NJ, 2016, pp. 232–234.
[79] M. Kanskar, D. Botez, T. Earles, T. Goodnough, L.J. Mawst, E. Stiers, 73% CW power conversion efficiency at 50 W from 970nm diode laser bar, Electron. Lett. 41 (2005) 245–247.
[80] A. Knigge, G. Erbert, J. Jonsson, W. Pittroff, R. Staske, B. Sumpf, M. Weyers, G. Trankle, Passively cooled 940 nm laser bars with 73% wall-plug efficiency at 70 W and 25 °C, Electron. Lett. 41 (2005) 250–251.
[81] N.A. Pikhtin, S.O. Slipchenko, D.A. Vinokurov, M.A. Khomylev, I.S. Tarasov, 72% wallplug efficiency and 16W CW front facet output optical power from 100-μm-aperture laser diode, in: C. Denman, I. Sorokina (Eds.), Advanced Solid-State Photonics (TOPS), Vol. 98 of OSA Trends in Optics and Photonics, Optical Society of America, 2005, p. 276.
[82] G. Erbert, F. Bugge, J. Fricke, P. Ressel, R. Staske, B. Sumpf, H. Wenzel, M. Weyers, G. Trankle, High-power high-efficiency 1150-nm quantum-well laser, IEEE J. Sel. Top. Quant. Electron. 11 (2005) 1217.
[83] N. Tansu, J.Y. Yeh, L.J. Mawst, Extremely-low threshold-current-density InGaAs quantum well lasers with emission wavelength of 1215-1233 nm, Appl. Phys. Lett. 82 (2003) 4038–4040.
[84] S. Mogg, N. Chitica, R. Schatz, R. Hammar, Properties of highly strained InGaAs/GaAs quantum wells for 1.2-μm laser diodes, Appl. Phys. Lett. 81 (2002) 2334–2336.
[85] P. Sundgren, J. Berggren, P. Goldman, M. Hammar, Highly strained InGaAs/GaAs multiple quantum-wells for laser applications in the 1200–1300 nm wavelength regime, Appl. Phys. Lett. 87 (2005), 071104.
[86] T. Takeuchi, Y.-L. Chang, A. Tandon, D. Bour, S. Corzine, R. Twist, M. Tan, H.-C. Luan, Low threshold 1.2 μm InGaAs quantum well lasers grown under low As/III ratio, Appl. Phys. Lett. 80 (2002) 2445–2447.
[87] F. Bugge, G. Erbert, J. Fricke, S. Gramlich, R. Staske, H. Wenzel, U. Zeimer, M. Weyers, 12 W continuous-wave diode lasers at 1120 nm with InGaAs quantum wells, Appl. Phys. Lett. 79 (2001) 1965–1967.
[88] T. Kondo, D. Schlenker, T. Miyamoto, Z. Chen, M. Kawaguchi, E. Gouardes, F. Koyama, K. Iga, Lasing characteristics of 1.2 μm highly strained GaInAs/GaAs quantum well lasers, Jpn. J. Appl. Phys. 40 (2000) 467–471.
[89] W.C. Chen, Y.K. Su, R.W. Chuang, H.C. Yu, M.C. Tsai, K.Y. Cheng, J.B. Horng, C. Hu, S. Tsau, Highly strained 1.22-μm InGaAs lasers grown by MOVPE, IEEE Photon. Technol. Lett. 26 (2008) 264–266.
[90] P.M. Ilroy, A. Kurobe, Y. Uematsu, Analysis and application of theoretical gain curves to the design of multi-quantum-well lasers, IEEE J. Quant. Electron. 21 (1985) 1958–1963.
[91] T.A. DeTemple, C.M. Herzinger, On the semiconductor laser logarithmic gain-current density relation, IEEE J. Quant. Electron. 29 (1993) 1246.
[92] G. Tsvid, J. Kirch, L. J. Mawst, M. Kanskar, J. Cai, R. A. Arif, N. Tansu, P. M. Smowton, and P. Blood, Radiative efficiency of InGaAs/InGaAsP/GaAs quantum well lasers, in LEOS 2007 - IEEE Lasers and Electro-Optics Society Annual Meeting Conference Proceedings.
[93] E. Yablonovitch, E.O. Kane, Reduction of lasing threshold current-density by the lowering of valence band effective mass, J. Lightwave Technol. 4 (1986) 504–506.
[94] A.R. Adams, Band-structure engineering for low-threshold high-efficiency semiconductor lasers, Electron. Lett. 22 (1986) 249–250.
[95] P. Blood, G.M. Lewis, P.M. Smowton, H. Summers, J. Thomson, J. Lutti, Characterization of semiconductor laser gain media by the segmented contact method, IEEE J. Sel. Top. Quant. Electron. 9 (2003) 1275–1282.
[96] L.J. Mawst, A. Bhattacharya, J. Lopez, D. Botez, D.Z. Garbuzov, L. DeMarco, J.C. Connolly, M. Jansen, F. Fang, R.F. Nabiev, 8 w continuous wave front-facet power from broad-waveguide al-free 980 nm diode lasers, Appl. Phys. Lett. 69 (1996) 1532–1534.
[97] G. Tsvid, J. Kirch, L.J. Mawst, M. Kanskar, J. Cai, R.A. Arif, N. Tansu, P.M. Smowton, P. Blood, Spontaneous radiative efficiency and gain characteristics of strained layer InGaAs/GaAs quantum well lasers, IEEE J. Quant. Electron. 44 (2008) 732–739.
[98] J.R. Meyer, C.A. Hoffman, F.J. Bartoli, L.R. Ram-Mohan, Type-II quantum-well lasers for the mid-wavelength infrared, Appl. Phys. Lett. 67 (1995) 757–759.
[99] R.Q. Yang, Infrared laser based on intersubband transitions in quantum wells, Superlattice. Microst. 17 (1995) 77–83.
[100] C.-H. Lin, R.Q. Yang, D. Zhang, S.J. Murry, S.-S. Pei, A.A. Allerman, S.R. Kurtz, Type-II interband quantum cascade laser at 3.8μm, Electron. Lett. 33 (1997) 598–599.
[101] C.L. Canedy, M.V. Warren, C.D. Merritt, W.W. Bewley, C.S. Kim, M. Kim, I. Vurgaftman, J.R. Meyer, Interband cascade lasers with longer wavelengths, Proc. SPIE 10111, Quantum Sensing and Nano Electronics and Photonics XIV (2017) 101110G.
[102] Anne Schade, Sven Höfling, Long wavelength interband cascade lasers on GaSb substrates, Proc. SPIE 10403, Infrared Remote Sensing and Instrumentation XXV (2017) 1040305.
[103] W.W. Bewley, J.R. Lindle, C.S. Kim, M. Kim, C.L. Canedy, I. Vurgaftman, J.R. Meyer, Lifetimes and auger coefficients in type-II "W" interband cascade lasers, Appl. Phys. Lett. 93 (2008), 041118.
[104] B.E. Hawkins, A.A. Khandekar, J.Y. Yeh, L.J. Mawst, T.F. Kuech, Effects of Gas switching sequences on GaAs/$GaAs_{1-y}Sb_y$ superlattices, J. Cryst. Growth 272 (2004) 686–693.
[105] M.J. Cherng, G.G. Stringfellow, R.M. Cohen, Organometallic vapor phase epitaxial growth of $GaAs_{0.5}Sb_{0.5}$, Appl. Phys. Lett. 44 (1984) 677.
[106] T.F. Kuech, S.E. Babcock, L.J. Mawst, Growth far from equilibrium: examples from III-V semiconductors, Appl. Phys. Rev. 3 (2016), 040801.
[107] M. Peter, R. Kiefer, F. Fuchs, N. Herres, K. Winkler, K.-H. Bachem, J. Wagner, Light-emitting diodes and laser diodes based on a $Ga_{1-x}In_xAs/GaAs_{1-y}Sb_y$ type II superlattice on InP substrate, Appl. Phys. Lett. 74 (1999) 1951–1953.
[108] J.Y.T. Huang, L.J. Mawst, T.F. Kuech, X. Song, S.E. Babcock, C.S. Kim, I. Vurgaftman, J.R. Meyer, A.L. Holmes Jr., Design and characterization of strained InGaAs/GaAsSb type-II 'W' quantum wells on InP substrates for mid-IR emission, J. Phys. D Appl. Phys. 42 (2009), 025108.

[109] S. Sprengel, A. Andrejew, K. Vizbaras, T. Gruendl, K. Geiger, G. Boehm, C. Grasse, M.-C. Amann, Type-II InP-based lasers emitting at 2.55 μm, Appl. Phys. Lett. 100 (2012), 041109.
[110] P. Dowd, W. Braun, D.J. Smith, C.M. Ryu, C.Z. Guo, S.L. Chen, U. Koelle, S.R. Johnson, Y.H. Zhang, Long wavelength (1.3 and 1.5 μm) photoluminescence from InGaAs/GaPAsSb quantum wells grown on GaAs, Appl. Phys. Lett. 75 (1999) 1267.
[111] M. Kudo, K. Ouchi, J.I. Kasai, T. Mishima, Low-lattice-strain long-wavelength GaAsSb/GaInAs type-II quantum wells grown on GaAs substrates, Jpn. J. Appl. Phys. 41 (2002) L1040.
[112] S.W. Ryu, P.D. Dapkus, Room temperature operation of type-II GaAsSb/InGaAs quantum well laser on GaAs substrates, Electron. Lett. 38 (2002) 564–565.
[113] C. Fuchs, A. Brüggemann, M.J. Weseloh, C. Berger, C. Möller, S. Reinhard, J. Hader, J.V. Moloney, A. Bäumner, S.W. Koch, W. Stolz, High-temperature operation of electrical injection type-II (GaIn)As/Ga(AsSb)/(GaIn)As "W"-quantum well lasers emitting at 1.3 μm, Sci. Rep. 8 (2018) 1422.
[114] N. Tansu, L.J. Mawst, Design analysis of 1550-nm GaAsSb-(In)GaAsN type-II quantum well laser active regions, IEEE J. Quant. Electron. 39 (2003) 1205–1210.
[115] I. Vurgaftman, J.R. Meyer, N. Tansu, L.J. Mawst, InP-based dilute-nitride mid-IR type-II "W" QW lasers, J. Appl. Phys. 96 (2004) 4653.
[116] L.J. Mawst, J.Y.T. Huang, D.P. Xu, T.F. Kuech, N. Tansu, MOCVD grown dilute-nitride type-II QWs, IEEE J. Sel. Top. Quant. Electron. 14 (2008) 979–991.
[117] M.K. Rathi, A.A. Khandekar, X. Song, S.E. Babcock, L.J. Mawst, T.F. Kuech, High antimony content $GaAs_{1-z}N_z$-$GaAs_{1-y}Sb_y$ type-II 'W' structure for long wavelength emission, J. Appl. Phys. 106 (2009), 063713.
[118] L. Yue, Y. Song, X. Chen, Q. Chen, W. Pan, X. Wu, J. Liu, L. Zhang, J. Shao, S. Wang, Novel type II InGaAs/GaAsBi quantum well for longer wavelength emission, J. Alloys Compd. 695 (2017) 753–759.
[119] C.A. Broderick, S. Jin, I.P. Marko, K. Hild, P. Ludewig, Z.L. Bushell, W. Stolz, J.M. Rorison, E.P. O'Reilly, K. Volz, S.J. Sweeney, $GaAs_{1-x}Bi_x/GaN_yAs_{1-y}$ type-II quantum wells: novel strain-balanced heterostructures for GaAs-based near- and mid-infrared photonics, Sci. Rep. 7 (2017) 46371.
[120] A.G. Norman, G.R. Booker, Transmission electron microscope and transmission electron diffraction observations of alloy clustering in liquid-phase epitaxial (001) GaInAsP layers, J. Appl. Phys. 57 (1985) 4715.
[121] K. Woodbridge, P. Blood, E.D. Fletcher, P.J. Huyler, Short wavelength (visible) GaAs quantum well lasers grown by molecular beam epitaxy, Appl. Phys. Lett. 45 (1984) 16–18.
[122] L.J. Mawst, M.E. Givens, C.A. Zmudzinski, M.A. Emanuel, J.J. Coleman, Optimization and characterization of index-guided visible AlGaAs/GaAs graded barrier quantum well laser diodes, IEEE J. Quant. Electron. 23 (1987) 696–703.
[123] M.A. Emanuel, J.A. Skidmore, M. Jansen, R. Nabiev, High-power InAlGaAs-GaAs laser diode emitting near 731 nm, IEEE Photon. Technol. Lett. 9 (1997) 1451–1453. Member.
[124] J.S. Roberts, J.P.R. David, L. Smith, P.L. Tihanyi, The influence of trimethylindium impurities on the performance of InAlGaAs single quantum well lasers, J. Cryst. Growth 195 (1998) 668–675.
[125] J.R. Shealy, High-efficiency superlattice graded-index separate confining heterostructure lasers with AlGaAs single quantum wells, Appl. Phys. Lett. 52 (1987) 1455–1457.
[126] P.L. Tihanyi, F.C. Jain, M.J. Robinson, J.E. Dixon, J.E. Williams, K. Meehan, M.S. O'Neill, L.S. Heath, D.M. Beyea, High power AlGaAs-GaAs visible diode lasers, IEEE Photon. Technol. Lett. 6 (1994) 775–777.
[127] R. Schatz, C.G. Bethea, Steady state model for facet heating leading to thermal runaway in semiconductor lasers, J. Appl. Phys. 76 (1994) 2509.
[128] K. Shigihara, Y. Nagai, S. Karakida, A. Takami, Y. Kokubo, H. Matsubara, S. Kakimoto, High-power operation of broad-area laser diodes with GaAs and AlGaAs single quantum wells for Nd:YAG laser pumping, IEEE J. Quant. Electron. 27 (1991) 1537.
[129] R.M. Lammert, G.M. Smith, D.V. Forbes, M.L. Osowski, J.J. Coleman, Strained-layer InGaAs-GaAs-AlGaAs buried-heterostructure lasers with nonabsorbing mirrors by selective-area MOCVD, Electron. Lett. 31 (1995) 1070–1072.
[130] S. Takahashi, T. Kobayashi, H. Saito, Y. Furukawa, GaAs–AlGaAs DH lasers with buried facet, Jpn. J. Appl. Phys. 17 (1978) 865–870.
[131] H. Yonezu, M. Ueno, T. Kamejima, I. Hayashi, An AlGaAs window structure laser, IEEE J. Quant. Electron. 15 (1979) 775–781.
[132] D. Botez, J.C. Connelly, Nonabsorbing-mirror (NAM) CDH-LOC diode lasers, Electron. Lett. 20 (1984) 530–532.
[133] C.L. Walker, A.C. Bryce, J.H. Marsh, Improved catastrophic optical damage level from laser with nonabsorbing mirrors, IEEE Photon. Technol. Lett. 14 (2002) 1394–1396.
[134] M. Gasser and E. E. Latta, Method for mirror passivation of semiconductor laser diodes, U.S. Patent 5 144 634, Sep. 1, 1992..
[135] J.S. Roberts, J.P.R. David, T.E. Sale, P. Tihanyi, High purity AlGaAs from methyl-based precursors using in situ gettering of alkoxides, J. Cryst. Growth 143 (1994) 135–140.
[136] R. Singh, D. Bull, F.P. Dabkowski, E. Clausen, A.K. Chin, High-power, reliable operation of 730 nm AlGaAs laser diodes, Appl. Phys. Lett. 75 (1999) 2002.
[137] S. Rusli, A. Al-Muhanna, T. Earles, L.J. Mawst, 1 W CW reliable λ=730 nm aluminium-free active layer diode laser, Electron. Lett. 36 (2000) 630–631.
[138] B. De Cremoux, P. Hirth, J. Ricciardi, On the presence of a solid immiscibility domain in the GaInAsP phase diagram, Inst. Phys. Conf. 56 (1981) 115–124.
[139] G.B. Stringfellow, Miscibility gaps in quaternary III/V alloys, J. Cryst. Growth 58 (1982) 194–202.
[140] S. Tanaka, K. Hiramatsu, Y. Habu, N. Sawaki, I. Akasaki, The initial stage of LPE growth of InGaAsP on GaAs in the region of immiscibility, J. Cryst. Growth 79 (1986) 978–983.
[141] K. Ono, M. Takemi, Anomalous behavior of phase separation of InGaAsP on GaAs substrates grown by MOVPE, J. Cryst. Growth 298 (2007) 41–45.
[142] M. Ohkubo, T. Ijichi, A. Iketani, T. Kikuta, 980-nm aluminum-free InGaAs/InGaAsP/InGaP GRIN-SCH SL-QW lasers, IEEE J. Quant. Electron. 30 (1994) 408.
[143] Y. Konaka, K. Ono, Y. Terai, Y. Fujiwara, Coexistence properties of phase separation and CuPt-ordering in InGaAsP grown on GaAs substrates by organometallic vapor phase epitaxy, J. Cryst. Growth 312 (2010) 2056–2059.
[144] L.J. Mawst, S. Rusli, A. Al-Muhanna, J.K. Wade, Short-wavelength (0.7 μm $< \lambda <$ 0.78 μm) high-power InGaAsP-active diode lasers, IEEE J. Sel. Top. Quant. Electron. 5 (1999) 785–791.
[145] R. Oshima, R.M. France, J.F. Geisz, A.G. Norman, M.A. Steiner, Growth of lattice-matched GaInAsP grown on vicinal GaAs(001) substrates within the miscibility gap for solar cells, J. Cryst. Growth 458 (2017) 1–7.
[146] D.P. Bour, D.W. Treat, K.J. Beernink, R.L. Thornton, T.L. Paoli, R.D. Bringans, Tensile-strained AlGaAsP and InGaAsP-$(AlGa)_{0.5}In_{0.5}P$ quantum well laser diodes for TM-mode emission in the wavelength range 650 $< \lambda <$ 850 nm, IEEE Photon. Technol. Lett. 6 (1994) 1283–1285.
[147] G. Erbert, F. Bugge, A. Knauer, J. Sebastian, A. Thies, H. Wenzel, M. Weyers, G. Trankle, High-power tensile-strained GaAsP-AlGaAs quantum-well lasers emitting between 715 and 790 nm, IEEE J. Sel. Top. Quant. Electron. 5 (1999) 780–784.
[148] J. Sebastian, G. Beister, F. Bugge, F. Buhrandt, G. Erbert, H.G. Hänsel, R. Hülsewede, A. Knauer, W. Pittroff, R. Staske, M. Schröder, H. Wenzel, M. Weyers, G. Tränkle, High-power 810-nm GaAsP–AlGaAs diode lasers with narrow beam divergence, IEEE J. Sel. Top. Quant. Electron. 7 (2001) 334–339.
[149] B. Sumpf, G. Beister, G. Erbert, J. Fricke, A. Knauer, W. Pittroff, P. Ressel, J. Sebastian, H. Wenzel, G. Trankle, 2W reliable operation of λ = 735 nm GaAsP/AlGaAs laser diodes, Electron. Lett. 37 (2001) 351–353.
[150] S.L. Yellen, A.H. Shepard, C.M. Harding, J.A. Baumann, R.G. Waters, D.Z. Garbuzov, V. Pjataev, V. Kochergin, P.S. Zory, Dark-line-resistant, aluminum-free diode laser at 0.8 μm, IEEE Photon. Technol. Lett. 4 (1992) 1328–1330.
[151] E. Nomoto, T. Taniguchi, T. Ohtoshi, S. Sasaki, K. Saito, H. Hamada, H. Hara, 700-730 nm InGaAsP quantum well ridge-waveguide lasers, SPIE 6909, Novel In-Plane Semiconductor Lasers VII (2008) 69091C.
[152] M. Weyers, M. Sato, H. Ando, Red shift of photoluminescence and absorption in dilute GaAsN alloy layers, Jpn. J. Appl. Phys. 31 (1992) L853.
[153] M. Kondow, T. Kitatani, S. Nakatsuka, M.C. Larson, K. Nakahara, Y. Yazawa, M. Okai, K. Uomi, GaInNAs: a novel material for long-wavelength semiconductor lasers, IEEE J. Sel. Top. Quant. Electron. 3 (1997) 719–730.
[154] W. Shan, W. Walukiewicz, J.W. Ager III, E.E. Haller, J.F. Geisz, D.J. Friedman, J.M. Olson, S.R. Kurtz, Band Anticrossing in GaInNAs alloys, Phys. Rev. Lett. 82 (1999) 1221.
[155] R. Asomoza, V.A. Elyukhin, R. Pena-Sierra, Spinodal decomposition range of $In_xGa_{1-x}N_yAs_{1-y}$ alloys, Appl. Phys. Lett. 81 (2002) 1785.
[156] W. Li, M. Pessa, T. Ahlgren, J. Decker, Origin of improved luminescence efficiency after annealing of Ga(In)NAs materials grown by molecular-beam epitaxy, Appl. Phys. Lett. 79 (2001) 1094.

[157] L.J. Mawst, J.-Y. Yeh, T. Van Roy, N. Tansu, Characteristics of MOCVD-grown dilute-nitride quantum well lasers, Proc. SPIE 5738, Novel In-Plane Semiconductor Lasers IV (2005).
[158] A.J. Ptak, S.W. Johnston, S. Kurtz, D.J. Friedman, W.K. Metzger, A comparison of MBE- and MOCVD-grown GaInNAs, J. Cryst. Growth 251 (2003) 392–398.
[159] O. Reentilä, M. Mattila, L. Knuuttila, T. Hakkarainen, M. Sopanen, H. Lipsanen, Comparison of H_2 and N_2 as carrier gas in MOVPE growth of InGaAsN quantum wells, J. Cryst. Growth 298 (2007) 536–539.
[160] A. Janotti, S.-H. Wei, S.B. Zhang, S. Kurtz, C.G. Van de Walle, Interactions between nitrogen, hydrogen, and gallium vacancies in $GaAs_{1-x}N_x$ alloys, Phys. Rev. B 67 (2003) 161201.
[161] K. Volz, D. Lacknera, I. Nemeth, B. Kunert, W. Stolz, C. Baur, F. Dimroth, A.W. Bett, Optimization of annealing conditions of (GaIn)(NAs) for solar cell applications, J. Cryst. Growth 310 (2008) 2222–2228.
[162] K. Volz, T. Torunski, W. Stolz, Detection of nanometer-sized strain fields in (GaIn)(NAs) alloys by specific dark field transmission electron microscopic imaging, J. Appl. Phys. 97 (2005), 014306.
[163] R. Oshima, J.Y. Huang, N. Miyashita, K. Matsubara, Y. Okada, F.A. Ponce, Transmission electron microscopy study of GaInNAs(Sb) thin films grown by atomic hydrogen-assisted molecular beam epitaxy, Appl. Phys. Lett. 99 (2011) 191907.
[164] K. Volz, T. Torunski, B. Kunert, O. Rubel, S. Nau, S. Reinhard, W. Stolz, Specific structural and compositional properties of (GaIn)(NAs) and their influence on optoelectronic device performance, J. Cryst. Growth 272 (2004) 739–747.
[165] T. Kim, L.J. Mawst, Y. Kim, K. Kim, J. Lee, T.F. Kuech, 13.2% efficiency double-hetero structure single-junction InGaAsN solar cells grown by MOVPE, J. Vac. Sci. Technol., A 33 (2015), 021205.
[166] N. Tansu, A. Quandt, M. Kanskar, W. Mulhearn, L.J. Mawst, High-performance and high-temperature continuous-wave-operation 1300 nm InGaAsN quantum well lasers by organometallic vapor phase epitaxy, Appl. Phys. Lett. 83 (2003) 18–20.
[167] D.A. Livshits, A.Yu Egorov, H. Riechert, 8 W continuous wave operation of InGaAsN lasers at 1.3 μm, Electron. Lett. 36 (2000) 1381–1382.
[168] G.L. Belenky, C.L. Reynolds, D.V. Donetsky, G.E. Shtengel, M.S. Hybertsen, M.A. Alam, G.A. Baraff, R.K. Smith, R.F. Kazarinov, J. Winn, L.E. Smith, Role of p-doping profile and regrowth on the static characteristics of 1.3-μm MQW InGaAsP-InP lasers: experiment and modeling, IEEE J. Quant. Electron. 35 (1999) 1515–1520.
[169] S.R. Bank, M. Wistey, L. Goddard, H. Yuen, H. Bae, J.S. Harris Jr., High-performance 1.5 μm GaInNAsSb lasers grown on GaAs, Electron. Lett. 40 (2004) 1186.
[170] G. Jaschke, R. Averbeck, L. Geelhaar, H. Riechert, Low threshold InGaAsN/GaAs lasers beyond 1500 nm, J. Cryst. Growth 278 (2005) 224–228.
[171] T. Garrod, D. Olson, M. Klaus, C. Zenner, C. Galstad, L. Mawst, D. Botez, 50% continuous-wave wallplug efficiency from 1.53μm-emitting broad-area diode lasers, Appl. Phys. Lett. 105 (2014), 071101.
[172] N. Tansu, L.J. Mawst, The role of hole leakage in 1300-nm InGaAsN quantum-well lasers, Appl. Phys. Lett. 82 (2003) 1500.
[173] R. Fehse, S. Tomic, A.R. Adams, S.J. Sweeney, E.P. O'Reilly, A. Andreev, H. Riechert, A quantitative study of radiative, Auger, and defect related recombination processes in 1.3-μm GaInNAs-based quantum-well lasers, IEEE J. Sel. Top. Quant. Electron. 8 (2002) 801–810.
[174] L. Shterengas, G. Belenky, J.Y. Yeh, L.J. Mawst, N. Tansu, Differential gain and linewidth-enhancement factor in dilute-nitride GaAs-based 1.3-μm diode lasers, IEEE J. Sel. Top. Quant. Electron. 11 (2005) 1063–1068.
[175] O. Anton, L.F. Xu, D. Patel, C.S. Menoni, J.Y. Yeh, T.T. Van Roy, L.J. Mawst, N. Tansu, The intrinsic frequency response of 1.3-μm InGaAsN lasers in the range T=10°C-80°C, IEEE Photon. Technol. Lett. 18 (2006) 1774.
[176] O.H. Anton, D. Patel, C.S. Menoni, J.-Y. Yeh, T.T. Van Roy, L.J. Mawst, J.M. Pikal, N. Tansu, Frequency response of strain-compensated InGaAsN-GaAsP-GaAs SQW lasers, IEEE J. Sel. Top. Quant. Electron. 11 (2005) 1079–1088.
[177] A. Belabbes, M. Ferhat, A. Zaoui, Giant and composition dependent optical bandgap bowing in dilute GaSbN alloys, Appl. Phys. Lett. 88 (2006) 152109.
[178] P.H. Jefferson, T.D. Veal, L.F.J. Piper, B.R. Bennett, C.F. McConville, B.N. Murdin, L. Buckle, G.W. Smith, T. Ashley, Band anticrossing in GaN_xSb_{1-x}, Appl. Phys. Lett. 89 (2006) 11129.
[179] W. Li, J.B. Heroux, W.I. Wang, InGaAsSbN: a dilute-nitride compound for midinfrared optoelectronic applications, J. Appl. Phys. 94 (2003) 4248.
[180] H. Benaissa, A. Zaoui, M. Ferhat, First principles calculations for dilute $InAs_{1-x}N_x$ alloys, J. Appl. Phys. 102 (2007) 113712.
[181] H.D. Sun, A.H. Clark, S. Calvez, M.D. Dawson, D.K. Shih, H.H. Lin, Photoluminescence characterization of midinfrared $InN_xAs_{1-x}/In_{0.53}Ga_{0.47}As/InP$ multiquantum wells with various N contents, Appl. Phys. Lett. 87 (2005), 081908.
[182] D.K. Shih, H.H. Lin, L.W. Sung, T.Y. Chu, T.R. Yang, Band gap reduction in InAsN alloys, Jpn. J. Appl. Phys. 42 (2003) 375.
[183] D.K. Shih, H.H. Lin, Y.H. Lin, $InAs_{0.97}N_{0.03}$/InGaAs/InP multiple quantum well lasers with emission wavelength λ = 2.38 μm, Electron. Lett. 37 (2001) 1342–1343.
[184] Q. Zhuang, A.M.R. Godenir, A. Krier, K.T. Lai, S.K. Haywood, Room temperature photoluminescence at 4.5 μm from InAsN, J. Appl. Phys. 103 (2008), 063520.
[185] Q. Zhuang, A. Godenir, A. Krier, Photoluminescence in InAsN epilayers grown by molecular beam epitaxy, J. Phys. D Appl. Phys. 41 (2008) 132002.
[186] J. Kirch, T.W. Kim, J. Konen, L.J. Mawst, T.F. Kuech, T.S. Kuan, Effects of antimony (Sb) incorporation on MOVPE grown $InAs_yP_{1-y}$ metamorphic buffer layers on InP substrates, J. Cryst. Growth 315 (2011) 96.
[187] J. Kirch, T. Garrod, S. Kim, J.H. Park, J.C. Shin, L.J. Mawst, T.F. Kuech, X. Song, S.E. Babcock, I. Vurgaftman, J.R. Meyer, T.-S. Kuan, $InAs_yP_{1-y}$ metamorphic buffer layers on InP substrates for mid-IR diode lasers, J. Cryst. Growth 312 (2010) 1165.
[188] R. Wheatley, M. Kesaria, L.J. Mawst, J.D. Kirch, T.F. Kuech, A. Marshall, Q.D. Zhuang, A. Krier, Extended wavelength mid-infrared photoluminescence from type-I InAsN and InGaAsN dilute nitride quantum wells grown on InP, Appl. Phys. Lett. 106 (2015) 232105.
[189] A. Beyer, W. Stolz, K. Volz, Metastable cubic zinc-blende III/V semiconductors: growth and structural characteristics, Prog. Cryst. Growth Char. 61 (2015) 46–62.
[190] M. Debbichi, A. Ben Fredj, A. Bhouri, M. Saïd, J.-L. Lazzari, Y. Cuminal, A. Joullié, P. Christol, Optical gain calculation of mid-infrared InAsN/GaSb quantum-well laser for tunable absorption spectroscopy applications, Mater. Sci. Eng. C 28 (2008) 751–754.
[191] C.A. Broderick, M. Usman, E.P. O'Reilly, Derivation of 12-and 14-band k·p Hamiltonians for dilute bismide and bismide-nitride semiconductors, Semicond. Sci. Technol. 28 (2013) 125025.
[192] S. Francoeur, M.-J. Seong, A. Mascarenhas, S. Tixier, M. Adamcyk, T. Tiedje, Band gap of $GaAs_{1-x}Bi_x$, $0< x< 3.6\%$, Appl. Phys. Lett. 82 (2003) 3874.
[193] K. Oe, H. Okamoto, New semiconductor alloy $GaAs_{1-x}Bi_x$ grown by metal organic vapor phase epitaxy, Jpn. J. Appl. Phys. 37 (1998) L1283.
[194] M. Usman, C.A. Broderick, Z. Batool, K. Hild, T.J.C. Hosea, S.J. Sweeney, E.P. O'Reilly, Impact of alloy disorder on the band structure of compressively strained $GaBi_xAs_{1-x}$, Phys. Rev. B 87 (2013) 115104.
[195] H. Jacobsen, B. Puchala, T.F. Kuech, D. Morgan, Ab initio study of the strain dependent thermodynamics of Bi doping in GaAs, Phys. Rev. B 86 (2012), 085207.
[196] S. Tixier, M. Adamcyk, T. Tiedje, S. Francoeur, A. Mascarenhas, P. Wei, F. Schiettekatte, Molecular beam epitaxy growth of $GaAs_{1-x}Bi_x$, Appl. Phys. Lett. 82 (2003) 2245–2247.
[197] K. Forghani, Y. Guan, A. Wood, S. Babock, L. Mawst, T.F. Kuech, The effect of the Bi precursors, $(CH_3)_3Bi$ and $(C_2H_5)_3Bi$, on the metal-organic vapor phase epitaxy of $GaAs_{1-y}Bi_y$ films, Chem. Vap. Depos. 21 (2015) 166–175.
[198] M. Kaminska, E.R. Weber, Z. Liliental-Weber, R. Leon, Z.U. Rek, Stoichiometry-related defects in GaAs grown by molecular-beam epitaxy at low temperatures, Vac. Sci. Technol. B 7 (1989) 710–713.
[199] H. Fushimi, K. Wada, Degradation mechanism in carbon-doped GaAs minority-carrier injection devices, IEEE Trans. Electron. Dev. 44 (1997) 1996–2001.
[200] P. Ludewig, N. Knaub, W. Stolz, K. Volz, MOVPE growth of Ga(AsBi)/GaAs multi quantum well structures, J. Cryst. Growth 370 (2013) 186–190.
[201] P. Ludewig, Z.L. Bushell, L. Nattermann, N. Knaub, W. Stolz, K. Volz, Growth of Ga(AsBi) on GaAs by continuous flow MOVPE, J. Cryst. Growth 396 (2014) 95–99.
[202] K. Forghani, Y. Guan, A.W. Wood, A. Anand, S.E. Babcock, L.J. Mawst, T.F. Kuech, Self-limiting growth when using trimethyl bismuth (TMBi) in the metal-organic vapor phase epitaxy (MOVPE) of $GaAs_{1-y}Bi_y$, J. Cryst. Growth 395 (2014) 38–45.
[203] H. Kim, K. Kim, Y. Guan, J. Lee, T.F. Kuech, L.J. Mawst, Single junction solar cell employing strain compensated $GaAs_{0.965}Bi_{0.035}/GaAs_{0.75}P_{0.25}$ multiple quantum wells grown by metal organic vapor phase epitaxy, Appl. Phys. Lett. 112 (2018) 251105.

[204] H. Kim, Y. Guan, S.E. Babcock, T.F. Kuech, L.J. Mawst, Characteristics of OMVPE grown GaAsBi QW lasers and impact of post-growth thermal annealing, J. Appl. Phys. 123 (2018) 113102.
[205] P. Ludewig, N. Knaub, N. Hossain, S. Reinhard, L. Nattermann, I.P. Marko, S.R. Jin, K. Hild, S. Chatterjee, W. Stolz, S.J. Sweeney, K. Volz, Electrical injection Ga (AsBi)/(AlGa) as single quantum well laser, Appl. Phys. Lett. 102 (2013) 242115.
[206] I.P. Marko, P. Ludewig, Z.L. Bushell, S.R. Jin, K. Hild, Z. Batool, S. Reinhard, L. Nattermann, W. Stolz, K. Volz, S.J. Sweeney, Physical properties and optimization of GaBiAs/(Al) GaAs based near-infrared laser diodes grown by MOVPE with up to 4.4% Bi, J. Phys. D Appl. Phys. 47 (2014) 345103.
[207] I.P. Marko, C.A. Broderick, S. Jin, P. Ludewig, W. Stolz, K. Volz, J.M. Rorison, E.P. O'Reilly, S.J. Sweeney, Optical gain in GaAsBi/GaAs quantum well diode lasers, Sci. Rep. 6 (2016) 28863.
[208] T. Fuyuki, R. Yoshioka, K. Yoshida, M. Yoshimoto, Long-wavelength emission in photo-pumped $GaAs_{1-x}Bi_x$ laser with low temperature dependence of lasing wavelength, Appl. Phys. Lett. 103 (2013) 202105.
[209] T. Fuyuki, K. Yoshida, R. Yoshioka, M. Yoshimoto, Electrically pumped room-temperature operation of $GaAs_{1-x}Bi_x$ laser diodes with low-temperature dependence of oscillation wavelength, APEX 7 (2014), 082101.
[210] I.P. Marko, S.R. Jin, K. Hild, Z. Batool, Z.L. Bushell, P. Ludewig, W. Stolz, K. Volz, R. Butkutė, V. Pačebutas, A. Geizutis, A. Krotkus, S.J. Sweeney, Properties of hybrid MOVPE/MBE grown GaAsBi/GaAs based near-infrared emitting quantum well lasers, Semicond. Sci. Technol. 30 (2015), 094008.
[211] R. Butkute, A. Geizutis, V. Pacebutas, B. Cechavicius, V. Bukauskas, R. Kundrotas, P. Ludewig, K. Volz, A. Krotkus, Multi-quantum well Ga(AsBi)/GaAs laser diodes with more than 6% of bismuth, Electron. Lett. 50 (2014) 1155.
[212] H. Kim, Y. Guan, K. Forghani, T.F. Kuech, L.J. Mawst, Laser diodes employing $GaAs_{1-x}Bi_x/GaAs_{1-y}P_y$ quantum well active regions, Semicond. Sci. Technol. 32 (2017), 075007.
[213] H. Kim, Y. Guan, T.F. Kuech, L.J. Mawst, Impact of thermal annealing on internal device parameters of $GaAs_{0.965}Bi_{0.035}/GaAs_{0.75}P_{0.25}$ quantum well lasers, IET Optoelectron. 13 (2018) 12–16.
[214] X. Wu, W. Pan, Z. Zhang, Y. Li, C. Cao, J. Liu, L. Zhang, Y. Song, H. Ou, S. Wang, 1.142 μm GaAsBi/GaAs quantum well lasers grown by molecular beam epitaxy, ACS Photonics 4 (2017) 1322–1326.
[215] H. Saito, K. Nishi, S. Sugou, Ground-state lasing at room temperature in long-wavelength InAs quantum-dot lasers on InP (311) B substrates, Appl. Phys. Lett. 78 (2001) 267–269.
[216] X. Han, H. Suzuki, J.-H. Lee, N. Kojima, Y. Ohshita, M. Yamaguchi, N incorporation and optical properties of GaAsN epilayers on (311) A/B GaAs substrates, J. Phys. D Appl. Phys. 44 (2010), 015402.
[217] M. Henini, J. Ibanez, M. Schmidbauer, M. Shafi, S.V. Novikov, L. Turyanska, S.I. Molina, D.L. Sales, M.F. Chisholm, J. Misiewicz, Molecular beam epitaxy of GaBiAs on (311) B GaAs substrates, Appl. Phys. Lett. 91 (2007) 251909.
[218] H. Kim, Novel III-V Active Regions by Metal-Organic Vapor Phase Epitaxy for Semiconductor Laser Diodes (Doctoral Dissertation, The University of Wisconsin-Madison, 2020.
[219] R. Teissier, D. Sicault, J.C. Harmand, G. Ungaro, G. Le Roux, L. Largeau, Temperature-dependent valence band offset and band-gap energies of pseudomorphic GaAsSb on GaAs, J. Appl. Phys. 89 (2001) 5473–5477.
[220] W. Pan, L. Zhang, L. Zhu, Y. Li, X. Chen, X. Wu, F. Zhang, J. Shao, S. Wang, Optical properties and band bending of InGaAs/GaAsBi/InGaAs type-II quantum well grown by gas source molecular beam epitaxy, J. Appl. Phys. 120 (2016) 105702.
[221] C.A. Broderick, S. Jin, I.P. Marko, K. Hild, P. Ludewig, Z.L. Bushell, W. Stolz, J.M. Rorison, E.P. O'Reilly, K. Volz, S.J. Sweeney, $GaAs_{1-x}Bi_x/GaN_yAs_{1-y}$ type-II quantum wells: novel strain-balanced heterostructures for GaAs-based near-and mid-infrared photonics, Sci. Rep. 7 (2017) 46371.